© 2019. Published by The Company of Biologists Ltd | Journal of Cell Science (2019) 132, jcs221655. doi:10.1242/jcs.221655

RESEARCH ARTICLE

The mitochondrial phosphatidylserine decarboxylase Psd1 is involved in nitrogen starvation-induced mitophagy in yeast

Pierre Vigié[1,2], Elodie Cougouilles[1,2], Ingrid Bhatia-Kiššová[3], Bénédicte Salin[1,2], Corinne Blancard[1,2] and Nadine Camougrand[1,2,*]

ABSTRACT

Mitophagy, the selective degradation of mitochondria by autophagy, is a central process that is essential for the maintenance of cell homeostasis. It is implicated in the clearance of superfluous or damaged mitochondria and requires specific proteins and regulators to perform. In yeast, Atg32, an outer mitochondrial membrane protein, interacts with the ubiquitin-like Atg8 protein, promoting the recruitment of mitochondria to the phagophore and their sequestration within autophagosomes. Atg8 is anchored to the phagophore and autophagosome membranes thanks to a phosphatidylethanolamine tail. In *Saccharomyces cerevisiae*, several phosphatidylethanolamine synthesis pathways have been characterized, but their contribution to autophagy and mitophagy are unknown. Through different approaches, we show that Psd1, the mitochondrial phosphatidylserine decarboxylase, is involved in mitophagy induction only after nitrogen starvation, whereas Psd2, which is located in vacuole, Golgi and endosome membranes, is required preferentially for mitophagy induction in the stationary phase of growth but also to a lesser extent for nitrogen starvation-induced mitophagy. Our results suggest that the mitophagy defect observed in Δ*psd1* yeast cells after nitrogen starvation may be due to a failure of Atg8 recruitment to mitochondria.

This article has an associated First Person interview with the first author of the paper.

KEY WORDS: Mitophagy, Phosphatidylethanolamine, Atg8 protein

INTRODUCTION

Autophagy is a cellular degradation process that is highly conserved among eukaryotic species by which cytosolic components such as organelles or proteins are degraded within specific compartments: the vacuole in yeast and plants, and lysosomes in mammalian cells. Autophagy can be split into three categories: microautophagy, chaperone-mediated autophagy (CMA) and macroautophagy (Jacob et al., 2017). Microautophagy occurs when vacuole membrane invagination sequesters organelles or proteins directly. CMA has been only characterized in mammalian cells and involves the recognition and translocation of protein substrates within the lysosomes (Tasset and Cuervo, 2016). Macroautophagy or bulk autophagy, commonly just called autophagy, requires transitory structures to be made (Feng et al., 2014). When this process is triggered, the phagophore, a membrane structure, appears from the phagophore-assembly site (PAS), located next to the vacuole in yeast. The phagophore elongates, closes, and forms an autophagosome, a vesicle containing sequestered cytosolic components. The autophagosome fuses with the vacuole membrane, releasing the cargo into the vacuolar lumen, where hydrolases degrade it. Degradation products are then exported to be reused by the cell. Many studies in yeast and mammalian cells have shown that different cellular compartments, such as mitochondria (Hailey et al., 2010), the Golgi (Van der Vaart et al., 2010), endoplasmic reticulum (ER) (Axe et al., 2008) and the plasma membrane (Ravikumar et al., 2010) may supply autophagosome membranes.

Defects in autophagy mechanisms or regulation have been linked to neurodegenerative diseases and cancers (Choi et al., 2013). The molecular mechanisms involved in autophagy have been widely studied, and this process has been increasingly understood both in yeast and mammalian cells. Autophagy requires more than 40 autophagy-related genes (denoted 'Atg') proteins. About 18 Atg proteins are part of the core autophagy machinery necessary to all types of autophagy, selective and non-selective, and the rest are implicated in selective types of autophagy processes (Wen and Klionsky, 2016). Bulk autophagy (hereafter referred to as autophagy) is considered a non-selective event; cytosolic components are sequestered within autophagosomes randomly. However, so far, many selective autophagic processes have been characterized. Peroxisomes, ribosomes, nucleus and mitochondria can be recruited to the PAS specifically and further degraded by autophagy (Suzuki, 2013). Autophagic degradation of mitochondria is called mitophagy and, in yeast, involves specific proteins. Atg32, an outer mitochondrial membrane protein, is the protein that marks mitochondria for degradation (Kanki et al., 2009a; Okamoto et al., 2009). Atg32 can interact with Atg8 (Okamoto et al., 2009), a protein whose phosphatidylethanolamine (PE) tail anchors it to the phagophore and autophagosome membranes (Ichimura et al., 2000). This interaction between Atg32 and Atg8 is responsible for the recruitment of mitochondria to the phagophore and for their further degradation within the vacuole. Depending on induction conditions, in addition to the interaction between Atg32 and Atg8, some other proteins are involved in mitophagy, including Atg11 (Kanki and Klionsky, 2008), Uth1 (Kissová et al., 2004), Aup1 (Tal et al., 2007), Atg33 (Kanki et al., 2009b), Whi2 (Mendl et al., 2011), Hog1, and Slt2 (Mao et al., 2011). PE has a central role in all autophagy processes because of its dual role in Atg8 lipidation and phagophore membrane elongation (Ichimura et al., 2000). PE is a major component of cell membranes, together with phosphatidylinositol (PI), phosphatidylserine (PS) and phosphatidylcholine (PC), in yeast (Klug and Daum, 2014). When non-selective and selective autophagy are triggered, the Atg8 ubiquitin-like conjugation system, involving Atg4, Atg7, and Atg3 proteins, lipidates Atg8 with PE

[1]CNRS, UMR5095, 1 rue Camille Saint-Saëns, 33077 Bordeaux, France. [2]Université de Bordeaux, UMR5095, 1 rue Camille Saint-Saëns, 33077 Bordeaux, France. [3]Comenius University, Faculty of Natural Sciences, Department of Biochemistry, Mlynská dolina CH1, 84215 Bratislava, Slovak Republic.

*Author for correspondence (n.camougrand@ibgc.cnrs.fr)

N.C., 0000-0002-7364-8962

Received 18 June 2018; Accepted 26 November 2018

Journal of Cell Science (2019) 132, jcs221655. doi:10.1242/jcs.221655

(Schlumpberger et al., 1997; Mizushima et al., 1998; Ichimura et al., 2000; Kirisako et al., 2000). In *Saccharomyces cerevisiae*, several PE synthesis pathways have been characterized to date (Fig. 1A). Mitochondria (Mito) and endoplasmic reticulum (ER) are the main compartments of PE production in yeast cells (Daum and Vance, 1997). Ept1, an ER-located enzyme, can perform *de novo* PE synthesis by converting cytidine-diphosphoethanolamine (CDP-Etn) into PE. CDP-Etn can be produced via both the Kennedy pathway from extracellular ethanolamine (Zelinski and Choy, 1982), and an enzymatic cascade involving Dpl1, which like Ept1, is also located in the ER. Two phosphatidylserine decarboxylases, Psd1 and Psd2, located in the inner mitochondrial membrane, and in the vacuole, Golgi and endosome (V/G/E) membranes, respectively, can also synthesize PE from phosphatidylserine (Trotter et al., 1993; Trotter and Woelker, 1995). Recently, the Nunnari laboratory have shown that Psd1 exhibits dual mitochondrial and ER localization, depending on the metabolic status of cells (Friedman et al., 2018). Reacylation of lyso-PE by Ale1 and Tgl3, in the ER and lipid droplets (LDs), respectively, constitutes the final pathway of PE synthesis (Calzada et al., 2016).

The central role of Atg8-PE in all nonselective and selective autophagy is now well established. However, the origin of PE required for autophagy and mitophagy induction is still unknown. In this work, we used mutants affected in single PE synthesis pathways to investigate the contribution of the different cellular PE pools on autophagy and mitophagy induction. Our results showed that, in yeast, mitochondrial phosphatidylserine decarboxylase 1 (Psd1) is involved in mitophagy only when nitrogen starvation induces the process.

RESULTS

Autophagy is not affected in deletion yeast strains defective in one PE synthesis pathway

Among all Atg proteins, Atg8 is particularly useful in the study of autophagy. This protein is located in the PAS and autophagosomal membranes, and is involved in autophagy process from the beginning to the end. To assess the role of each PE-producing enzyme in autophagy, we submitted BY4742 (wild-type, WT) and Δ*psd1*, Δ*psd2*, Δ*ale1*, Δ*ept1*, Δ*tgl3* and Δ*dpl1 S. cerevisiae* strains expressing GFP–Atg8 and grown on a strict respiratory carbon source to nitrogen starvation or harvested them after 1 day of

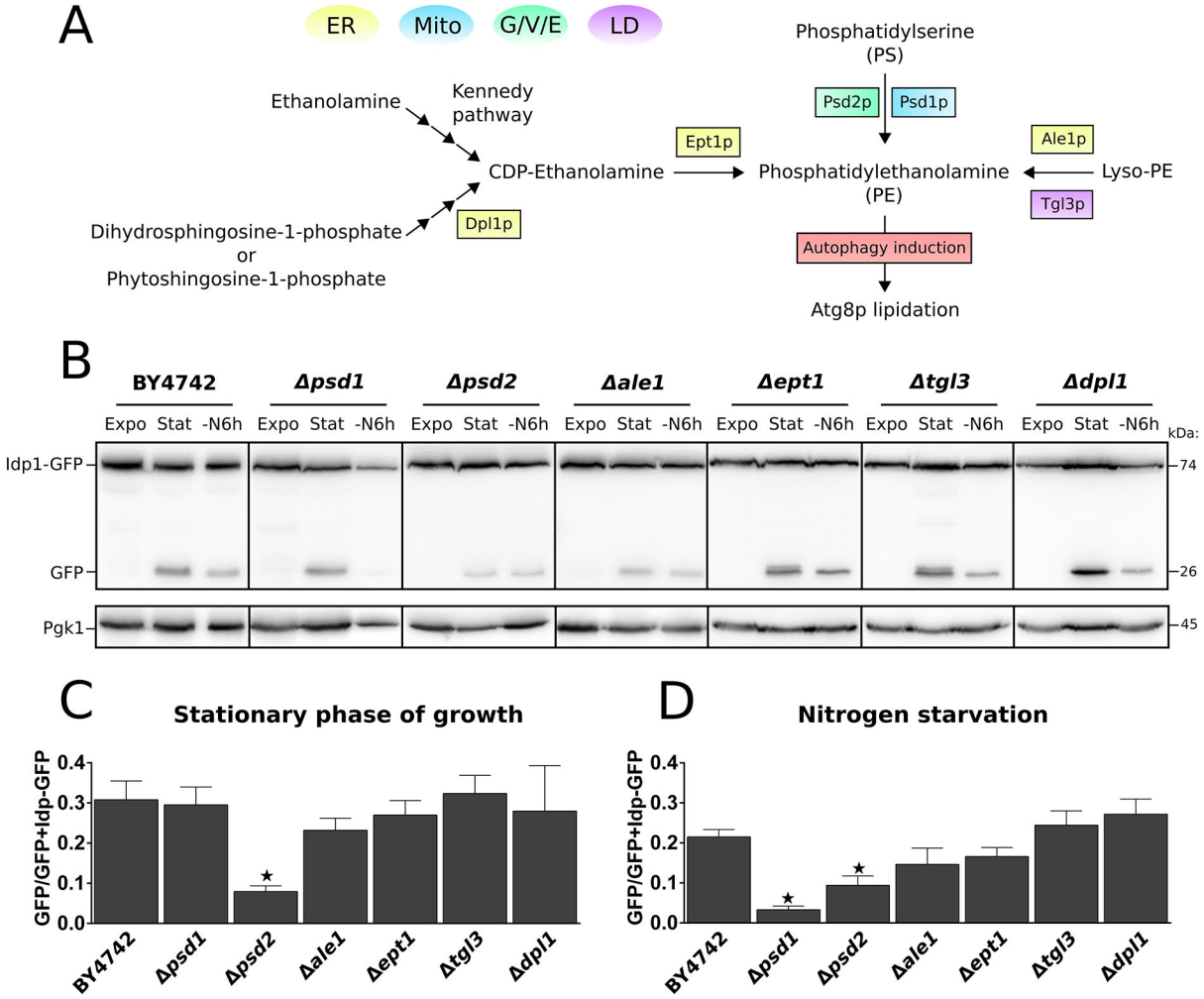

Fig. 1. The Δ*psd1* strain shows a defect in nitrogen starvation-induced mitophagy. (A) Pathways of PE synthesis in yeast. See text for details. (B) BY4742 (WT), Δ*psd1*, Δ*psd2*, Δ*ale1*, Δ*ept1*, Δ*tgl3* and Δ*dpl1* strains grown in a medium supplemented with a respiratory carbon source and expressing Idp1–GFP were submitted for 6 h of nitrogen starvation (–N6 h) or 1 day of stationary phase growth (Stat). Cells harvested in an exponential phase of growth (Expo) were used as negative control. Western blots and immunodetection were performed as described in the Materials and Methods. (C,D) Mitophagy induction was quantified as a ratio of GFP:(GFP+Idp1-GFP). **P*<0.05. Data are mean±s.e.m. and were obtained from at least five independent experiments for each tested strain.

Journal of Cell Science (2019) 132, jcs221655. doi:10.1242/jcs.221655

stationary phase growth. These conditions induce both autophagy and mitophagy in yeast (Bhatia-Kiššová and Camougrand, 2010). Under basal conditions, GFP–Atg8 is only located in the PAS, whereas under autophagy-inducing conditions, GFP–Atg8 is transported into the vacuolar lumen, where hydrolases degrade the Atg8 moiety more rapidly than GFP moiety. Next, we quantified autophagy induction from western immunoblot analyses by calculating the ratio of the amount of residual GFP to that of total GFP (GFP+GFP–Atg8). We observed no significant differences, even in the kinetics of autophagy implementation, between WT and all strains in which one PE synthesis pathway was impaired, both in the stationary phase of growth and after 6 h of nitrogen starvation, meaning that autophagy required no central PE enzyme in the conditions we used (Fig. S1A–K). Our results show that existing PE synthesis pathways can compensate for absent pathways.

Mitophagy requires different enzymes of PE synthesis depending on conditions of induction

We studied mitophagy induction in WT and Δ*psd1*, Δ*psd2*, Δ*ale1*, Δ*ept1*, Δ*tgl3* and Δ*dpl1* strains expressing Idp1–GFP. Under basal conditions, this fusion protein is only located in mitochondrial matrix. Under mitophagy-inducing conditions, mitochondria are sequestered within autophagosomes and degraded within the vacuole; consequently, residual GFP is detectable in this compartment. As for the autophagy experiments, mitophagy was induced either by 6 h of nitrogen starvation or after 1 day of stationary phase growth on a respiratory carbon source (Fig. 1B). We performed a quantification of western immunoblots (Fig. 1C,D) by measuring ratio of the amount of residual GFP to that of total GFP (GFP+Idp1-GFP). While mitophagy was not affected in Δ*ale1*, Δ*ept1*, Δ*tgl3* or Δ*dpl1* strains in the stationary phase of growth, we noticed a faint decrease in mitophagy in Δ*ale1* and Δ*ept1* strains during nitrogen starvation (Fig. 1B,D). Interestingly, we observed that Δ*psd1* and Δ*psd2* mutant strains, both deleted for a phosphatidylserine decarboxylase, exhibited different phenotypes. After 1 day in stationary phase growth, in comparison with WT, mitophagy induction was delayed in Δ*psd2* strain only, whereas after 6 h of nitrogen starvation, mitophagy was impaired in Δ*psd2* (45% of WT) and, to a greater extent in Δ*psd1* (15% of WT) strain (Fig. 1B–D). To quantify mitophagy, we performed measurements of mitoPho8Δ60 alkaline phosphatase (ALP) activity as described previously (Kanki et al., 2009b). Pho8 is a vacuolar alkaline phosphatase synthesized as an immature form in the cytosol and imported and matured within the vacuole. The truncated Pho8Δ60 version of this protein cannot be imported into the vacuolar lumen; by addressing this truncated protein to mitochondria, thanks to a *COXIV* mitochondrial-targeting sequence, mitophagy is the only way for this protein to be delivered to and matured in the vacuole. Thus, this assay is a very convenient tool for quantitative measurement of mitophagy. All strains displayed a basal level of mitoPho8Δ60-dependent alkaline phosphatase activity because of the presence of Pho13, another alkaline phosphatase (Fig. 2A,B). Nitrogen starvation treatment induced an increase in ALP activity in WT because of mitophagy induction (Fig. 2A). This activity was 40% lower in the Δ*psd1* strain and 25% lower in the Δ*psd2* strain than in WT. In the stationary phase of growth, the ALP activity increased in WT and in the Δ*psd1* strain and was lower in the Δ*psd2* strain (Fig. 2B). Cells lacking Atg32 protein (Δ*atg32*) cannot perform mitophagy in this condition, so we used them as a negative control. These results confirmed the findings from western immunodetection analyses, and suggest that during the beginning of nitrogen starvation, the presence of Psd1 is crucial for the induction of mitophagy and could provide PE to autophagy machinery to initiate mitochondrial degradation. The scenario is completely different in the stationary phase of growth, in which the activity of Psd2 is strictly necessary. We note that, in WT cells, nitrogen starvation does not change mitochondrial lipid composition compared to that seen during the exponential phase of growth (Fig. S2A–C). Finally, we performed immunoelectron microscopy on WT and Δ*psd1* strains. We prevented degradation of autophagic bodies (ABs) by addition of PMSF, as described previously (Kiššová et al., 2007) and compared the number of vesicles (ABs) in the vacuole and the number of cells with mitochondria within the vacuole. As expected, the number of cells with vacuole-containing mitochondria was much lower in the Δ*psd1* strain than in WT (Fig. 2C).

We next focused on mitochondrial Psd1, and, using different approaches, we confirmed that mitophagy impairment in Δ*psd1* strain is due to an absence of Psd1. The mitophagy defect was rescued in the Δ*psd1* strain expressing p*PSD1* after 6 h of nitrogen starvation, as shown by the appearance of free GFP in this strain on western blots to a similar level as observed in WT (Fig. 3A,B). Accordingly, the mitoPho8Δ60 alkaline phosphatase (ALP) activity defect was also rescued in Δ*psd1* strains expressing p*PSD1* (Fig. 2A). Psd2, which is located in membranes of the Golgi, vacuole and endosomes, is the other phosphatidylserine decarboxylase characterized in eukaryotes (Trotter and Woelker, 1995; Zinser et al., 1991; Riekhof et al., 2014; Gulshan et al., 2010). Overexpression of Psd2, in the Δ*psd1* strain, in which it localizes in the cytosol, rescued the observed defect in induction of mitophagy after nitrogen starvation (Fig. S3A). Surprisingly, no beneficial effect of overexpression of Psd2 was observed if protein was targeted to mitochondria. Because the Atg32 protein plays a crucial role during mitophagy by acting as a mitochondrial receptor for the autophagy machinery, we also checked whether the mitophagy defect in the Δ*psd1* strain was cause by an alteration in Atg32 expression. We tagged the C-terminus of Atg32 with a V5 tag and analyzed Atg32–V5 expression in both parental and Δ*psd1* strains during the exponential phase of growth and after 3 h of nitrogen starvation. We did not see any difference in Atg32 expression in these conditions in WT or Δ*psd1* strains. This result suggests that the mitophagy defect in the Δ*psd1* strain does not depend on the Atg32 protein expression (Fig. S3B,C).

Atg8 protein localizes to mitochondria under nitrogen starvation

Considering the importance of PE synthesized by mitochondrial Psd1 in mitophagy triggered by nitrogen starvation, we hypothesized that mitochondria could provide this phospholipid for Atg8 conjugation. To investigate this hypothesis, we isolated mitochondria from WT, Δ*psd1* and Δ*psd2* strains expressing GFP–Atg8 after 3 h of nitrogen starvation. We loaded purified mitochondria on sucrose gradients and, after centrifugation, collected and analyzed fractions by western immunodetection analyses. We were able to visualize GFP–Atg8 in fractions in which porin, a mitochondrial protein, was the most abundant, in all strains (Fig. 4A–C), which suggested recruitment of GFP–Atg8 to mitochondria. The GFP–Atg8:porin ratio was similar between WT and Δ*psd2* strains. However, this ratio decreased by 50% in Δ*psd1* compared with WT (Fig. 4D). In cell fractionation experiments, we detected ∼40% of GFP–Atg8 in mitochondrial fractions in WT cells and only ∼20% in the Δ*psd1* strain (Fig. S4A,B). When we isolated mitochondria from WT cells that were grown in the presence of glucose and submitted to nitrogen starvation, a

Journal of Cell Science (2019) 132, jcs221655. doi:10.1242/jcs.221655

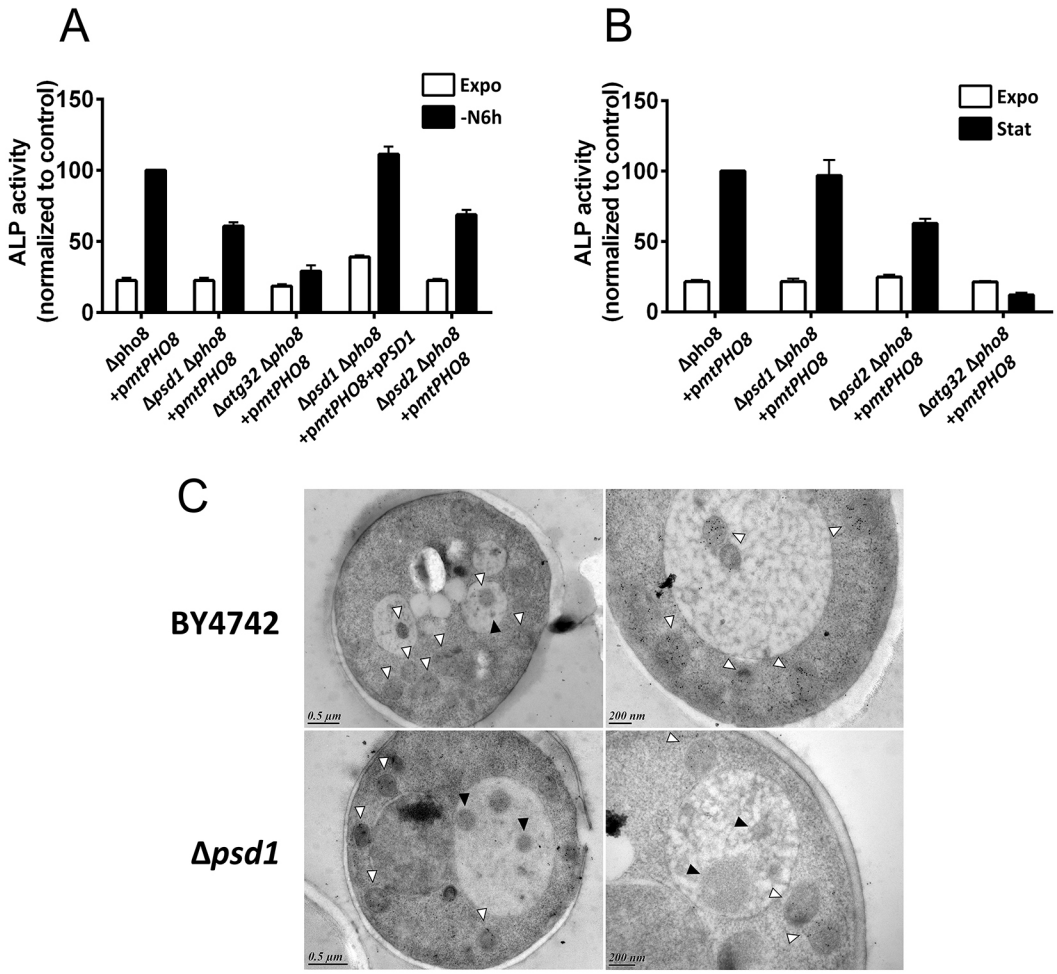

	Number of cells analyzed	Number of cells with vesicles in vacuoles	Number of cells with mitochondria in vacuoles
Wild-type	209	117 (56%)	70 (33.5%)
Δpsd1	116	76 (65.5%)	17 (14.6%)

Fig. 2. The *Δpsd1* strain shows a defect in nitrogen starvation-induced mitophagy. (A,B) Study of mitophagy by measuring the alkaline phosphatase (ALP) activity assay. BY4742 (WT), Δ*psd1*, Δ*atg32*, Δ*psd2* and Δ*psd1+pPSD1* strains grown in a medium supplemented with a respiratory carbon source and expressing mitochondria-targeted Pho8Δ60 (*pmtPHO8*), were harvested during the exponential phase of growth (Expo) and submitted either for (A) 6 h of nitrogen starvation (−N6 h) or (B) 1 day of stationary phase growth (Stat). Cells were lysed and ALP activity was determined as described in the Materials and Methods. Data are mean±s.e.m. for three independent experiments. (C) Immunoelectron microscopy on BY4742 and Δ*psd1* strains was carried out with antibodies targeting the mitochondrial outer membrane protein porin. Cells grown in a medium supplemented with a respiratory carbon source were harvested in an exponential phase of growth and then subjected to nitrogen starvation for 3 h in the presence of 1 mM PMSF. The pictures show a typical example of whole cell (left) or a detail (right) displaying vacuoles containing autophagic bodies (vesicles) or mitochondria for each strain. Black arrowheads represent vesicles and white arrowheads show gold-labeled mitochondria. The table shows differences in the number of cells containing vesicles and mitochondria between WT and Δ*psd1* strains.

condition in which mitophagy is not induced, we found no localization of GFP–Atg8 in mitochondrial fractions (Fig. S4C,D). Our results suggest that the mitophagy defect observed in the Δ*psd1* strain under nitrogen starvation conditions may be the result of failure to recruit Atg8 to the mitochondrial surface.

To further examine the nature of the association of Atg8 with mitochondria, we next treated mitochondria, purified from WT that had been exposed to 3 h of nitrogen starvation, with sodium carbonate and Triton X-100 (TX-100). GFP–Atg8 was detected in pellet fraction upon sodium carbonate treatment, and it was visualized in the supernatant when mitochondria were treated with TX-100 (Fig. S4E). This result suggests that GFP–Atg8 is a peripheral protein not only associated with mitochondrial membranes but also likely anchored to them owing to its PE moiety.

To confirm the localization of Atg8 to mitochondria upon nitrogen starvation, we also carried out an immunoelectron microscopy analysis with antibodies directed against the Atg8 protein. After 3 h of nitrogen starvation, we observed a significant number of WT cells with clusters of gold particles on the mitochondrial surface, autophagosomes and ABs. In the Δ*psd1*

Journal of Cell Science (2019) 132, jcs221655. doi:10.1242/jcs.221655

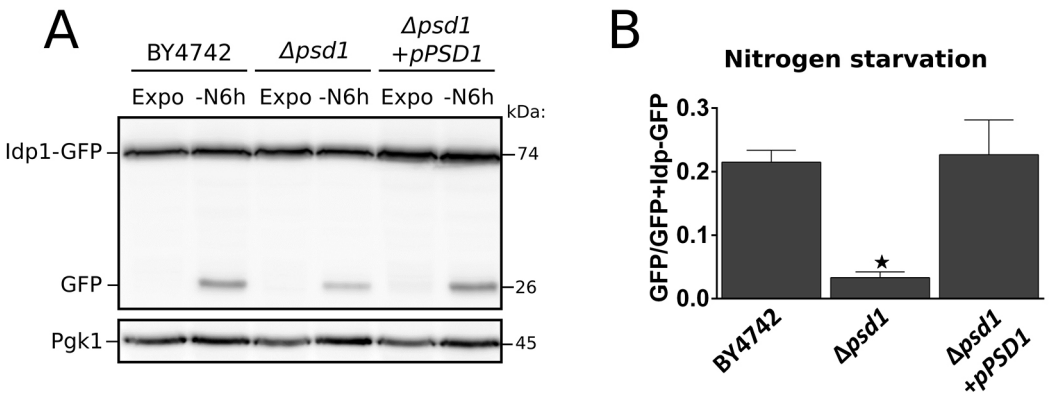

Fig. 3. The mitophagy defect in the Δ*psd1* strain is rescued by Psd1 reintroduction. (A) BY4742, Δ*psd1* and Δ*psd1*+p*PSD1* cells, grown in a medium supplemented with a respiratory carbon source and expressing Idp1–GFP were harvested in a mid-exponential phase of growth (Expo) or submitted for 6 h of nitrogen starvation (–N6 h). The protein extraction, western blotting and immunodetection were performed as described in the Materials and Methods. (B) Mitophagy induction was quantified as a ratio of GFP:(Idp1-GFP+GFP). **P*<0.05. Data are mean±s.e.m. for at least five independent experiments for each tested strain.

strain, Atg8 clusters on mitochondria were less frequent (20%) and much smaller than in WT cells (50%) (Fig. 5A–D). We also checked the localization of two proteins of the Atg8-conjugation machinery, Atg3 and Atg4, to mitochondria in nitrogen starvation. We performed cell fractionation on WT cells expressing Atg3–GFP and Atg4–GFP submitted to 3 h of nitrogen starvation, and we observed a very weak GFP signal in the mitochondrial fractions (fractions where porin is abundant) (Fig. S5A,B). In order to determine Atg3 and Atg4 localization more precisely, we prepared crude mitochondrial extracts from these two strains and loaded them on sucrose gradients. We detected Atg3–GFP and Atg4–GFP proteins in porin-enriched fractions (Fig. 6A,B). Moreover, we observed clusters of Atg4–GFP on mitochondria by immunoelectron microscopy (Fig. 6C). At the same time, we found Atg4 dispersed in cytosol, as expected based on its function in the process of Atg8 cleavage to a form required for autophagosome formation. In the stationary phase of growth, Atg4–GFP is not found in mitochondrial fractions (Fig. S5C). Our data suggest that Atg8 and Atg8-conjugation machinery could be recruited to mitochondria specifically in response to nitrogen starvation-induced mitophagy; thus, Atg8 can be conjugated to mitochondria directly.

We next wondered whether we could visualize Atg8 recruitment to mitochondria by fluorescence microscopy. We examined a WT strain expressing Ilv3–RFP (a mitochondrial matrix protein fused to RFP) and GFP–Atg8 submitted to nitrogen starvation. We were able to observe a few colocalization events between GFP–Atg8 and mitochondria, but they were very fast and transient (~4 min)

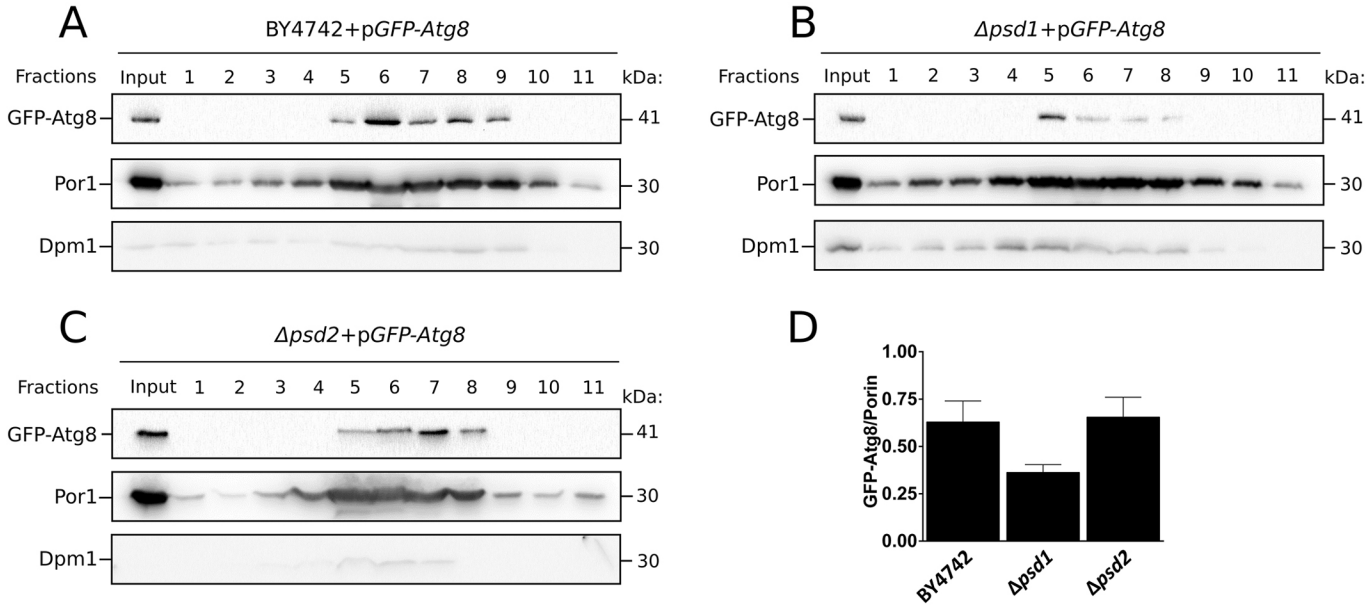

Fig. 4. GFP–Atg8 localization to mitochondria is impaired in Δ*psd1* cells. BY4742 (A), Δ*psd1* (B), Δ*psd2* (C) cells were grown in a medium supplemented with a respiratory carbon source and expressing a GFP–Atg8 fusion protein were harvested in a mid-exponential phase of growth and submitted for 3 h of nitrogen starvation. Crude mitochondrial extracts were prepared as described in the Materials and Methods. Mitochondria were loaded on top of a 20–60% sucrose gradient. After centrifugation, fractions were collected and analyzed by western blotting. For immunodetection, antibodies against GFP or porin (Por1) were used to detect the GFP–Atg8 fusion protein and mitochondria-containing fractions, respectively. The protein Dmp1 was used as a marker of the ER. (D) For each blot, GFP-Atg8:Por1 ratio was quantified from the fractions 5–8, in which (i) GFP–Atg8 was detected, and (ii) Por1 was the most abundant. Data are mean±s.e.m. for three independent experiments for each tested strain.

Journal of Cell Science (2019) 132, jcs221655. doi:10.1242/jcs.221655

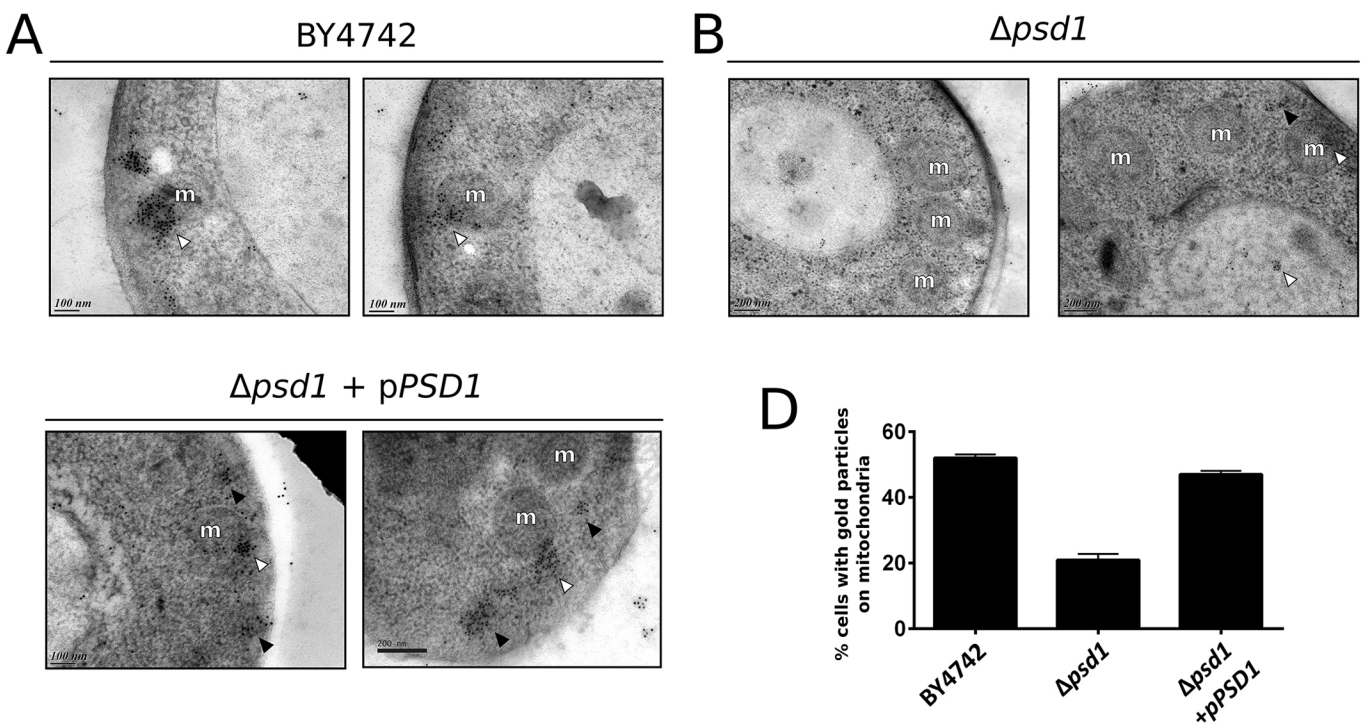

Fig. 5. Study of GFP-Atg8 mitochondrial localization by immunoelectron microscopy. BY4742 (A), Δ*psd1* (B) and Δ*psd1*+p*PSD1* (C) cells grown in a medium supplemented with a respiratory carbon source were submitted for 3 h of nitrogen starvation in the presence of 1 mM PMSF. Immunoelectron samples were prepared as described in the Materials and Methods. Anti-Atg8 antibodies were used to visualize endogenous Atg8 protein. White arrowheads represent gold-particle clusters on mitochondria; black arrowheads show gold-particle clusters on vesicles. M, mitochondria. (D) The quantification of cells containing gold-labeled mitochondria was determined in BY4742, Δ*psd1*, and Δ*psd1*+p*PSD1* strains. Data are mean±s.e.m. for three independent experiments. In each experiment, ∼200 cells for each strain were examined.

(Fig. 7A). Every acquisition was taken at a 2 min interval, enough for GFP–Atg8 to colocalize with and then not be retained on mitochondria. We had demonstrated previously that two waves of mitophagy occur in nitrogen starvation (Kiššová et al., 2007). In the first hours of nitrogen starvation, mitochondria are targeted selectively for degradation by autophagy machinery; later, mitochondria are degraded by general autophagy. We next wondered whether colocalization events between GFP–Atg8 and mitochondria would occur in close proximity to the vacuole, meaning that mitochondria located near to the vacuole would be degraded first by mitophagy. We carried out fluorescence microscopy in WT cells expressing Ilv3–RFP and GFP–Atg8 and with FM4-64-stained vacuoles. After 3 h of nitrogen starvation, colocalization between GFP–Atg8 and mitochondria occurred next to the vacuole (Fig. 7B), suggesting degradation of mitochondria in close proximity to this cell compartment.

DISCUSSION

Autophagy and mitophagy are two central processes required for cell homeostasis and survival. One step required for all general and selective autophagy processes is Atg8 (LC3 proteins are the mammalian Atg8 homologs) conjugation with PE, which is mediated by the Atg8-conjugation system (Ichimura et al., 2000; Kirisako et al., 2000). After PC, PE is the most abundant phospholipid in eukaryotic cells, and can be synthesized via different pathways in yeast (Fig. 1A). Among them, in standard culture condition, when cells are grown in a medium containing glucose as carbon source, the mitochondrial phosphatidylserine decarboxylase Psd1 synthesizes the majority of PE via decarboxylation of PS (Birner et al., 2001). Previous studies have shown that Psd1 is responsible for 85% of phosphatidylserine decarboxylase activity (Trotter et al., 1993). Moreover, PE content, measured in mitochondria isolated from cells grown in lactate as a carbon source, was 87% lower in the Δ*psd1* mutant than in WT (Storey et al., 2001). It was also shown that PE positively regulates autophagy and longevity (Rockenfeller et al., 2015). We used yeast strains with one impaired PE synthesis pathway (Δ*psd1*, Δ*psd2*, Δ*ept1*, Δ*ale1*, Δ*tgl3* and Δ*dlp1*) to assess the contribution of each pathway in autophagy induction. Our results showed no differences in autophagy induction, both in the stationary phase of growth and under nitrogen starvation, between WT and all mutants with a single impaired PE synthesis pathway, suggesting no central enzyme supplies PE to the autophagy machinery (Fig. S1). Our data also suggest that, in yeast cells, PE synthesis pathways can compensate for each other to supply PE to autophagy machinery in both conditions. These results suggest that the PE necessary for autophagy can come from different cellular compartments, and are in agreement with previous studies showing membranes required for autophagy can have different origins. Moreover, depletion of both pathways involving Psd1 and Psd2 has an impact on autophagy (Nebauer et al., 2007). Recently, the Nunnari laboratory reinvestigated Psd1 location and found that this protein is localized not only in mitochondria but also in ER, depending on the metabolic status of cells (Friedman et al., 2018). However, in their study, the authors did not discuss the possibility that the ER location of Psd1 could be related to mitochondrial-associated membranes (MAMs) derived from the ER. Bürgermeister et al. also observed that a certain portion of PE synthesized by Psd2 can be imported into mitochondria with a moderate efficiency (Bürgermeister et al., 2004). In addition, some data have suggested that autophagy

Journal of Cell Science (2019) 132, jcs221655. doi:10.1242/jcs.221655

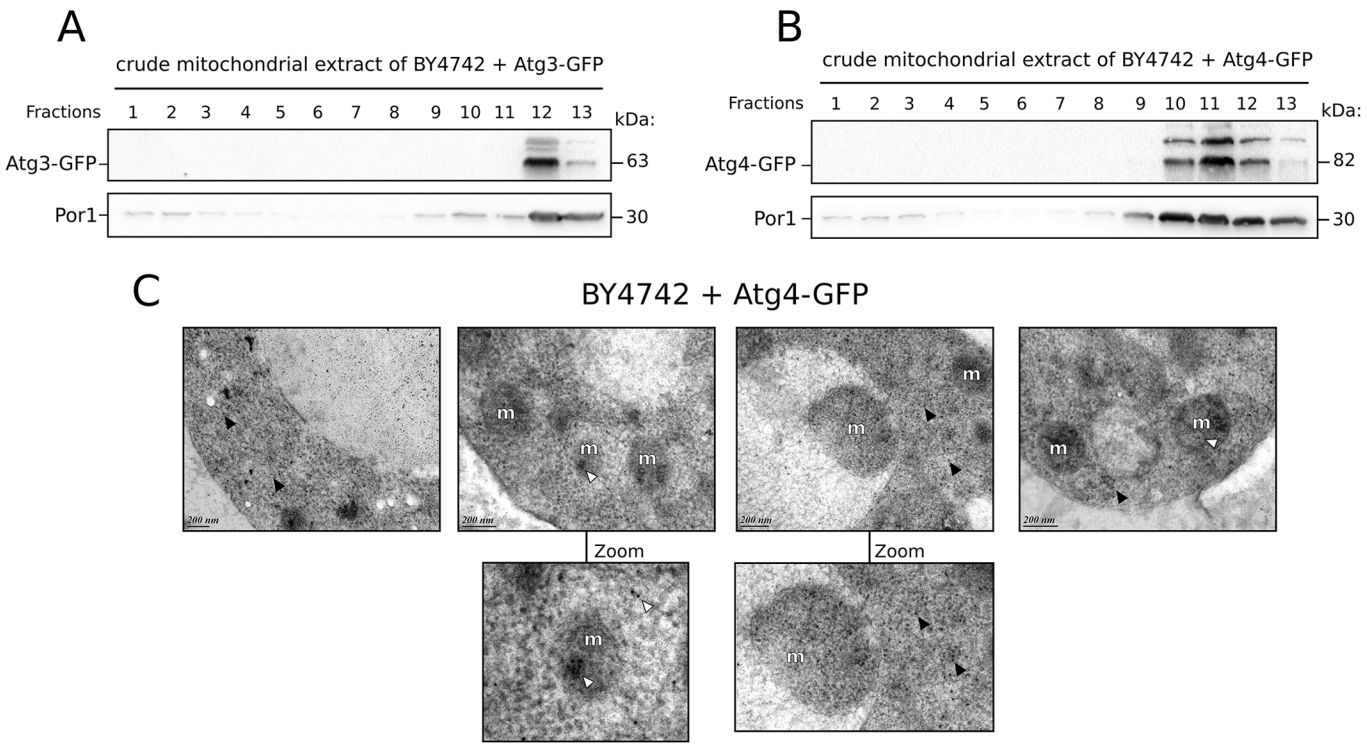

Fig. 6. Atg8-conjugation machinery proteins are located in mitochondria under nitrogen starvation. BY4742 cells expressing Atg3–GFP (A) or Atg4–GFP (B) grown in a medium supplemented with a respiratory carbon source were harvested in a mid-exponential phase of growth and submitted for 3 h of nitrogen starvation. Cell fractionation and mitochondria isolation were performed as described in the Materials and Methods. Mitochondria from the corresponding strains were loaded on top of a 20–55% sucrose gradient. After centrifugation, fractions were collected and analyzed by western blotting. Anti-GFP antibody was used to detect Atg3–GFP or Atg4–GFP proteins; anti-Por1 antibody was used to visualize mitochondria-containing fractions. (C) BY4742 cells expressing Atg4–GFP grown in a medium supplemented with a respiratory carbon source were harvested in a mid-exponential phase of growth and submitted for 3 h of nitrogen starvation in the presence of 1 mM PMSF. Then, immunoelectron microscopy was carried out as described in the Materials and Methods. Samples were incubated with anti-GFP antibody. White arrowheads represent gold-particle clusters on mitochondria; black arrowheads show gold particles in the cytosol; m, mitochondrion. The presented images were obtained from two independent experiments.

competes for a common PE pool with major cellular PE-consuming pathways, such as glycosylphosphatidylinositol anchoring (Wilson-Zbinden et al., 2015). Considering lipid trafficking and the major role of autophagy, our results are therefore not so surprising.

Considering mitophagy, Δ*psd1* or Δ*psd2* mutants exhibited an impairment of this process depending on conditions of induction. When we submitted cells to nitrogen starvation, mitophagy induction was impaired in the Δ*psd2* strain and by an even greater extent in the Δ*psd1* strain, whereas in the stationary phase of growth, mitophagy induction was impaired in the Δ*psd2* strain only (Fig. 1B–D). The mitochondrial localization of Psd2 (Bürgermeister et al., 2004) may help to explain the observation that mitophagy is also affected in the Δ*psd2* mutant during nitrogen starvation, but to a lesser extent than in the Δ*psd1* mutant. Unfortunately, we could not include the double-mutant Δ*psd1psd2* in our study because it does not grow in the medium we used containing lactate as respiratory carbon source, as previously shown by Daum laboratory (Horvath et al., 2011). Our data highlight the importance of phosphatidylserine decarboxylase activity in mitophagy induction in both conditions, but most importantly the requirement for Psd1 specifically in nitrogen starvation-induced mitophagy. Expression of Psd1 or overexpression of Psd2 were enough to rescue the impairment in mitophagy in the Δ*psd1* strain. Some proteins are known to be required only for mitophagy induced by stationary phase growth, such as Aup1 or Atg33 (Tal et al., 2007; Kanki et al., 2009b). Psd2 can now be added to this list. To our knowledge, Psd1 is the first protein shown to be strictly involved in nitrogen starvation-induced mitophagy. Our results also mean that mitochondria could supply PE for Atg8 lipidation or phagophore membrane elongation in order to promote their own degradation under nitrogen starvation. Immunoprecipitation experiments during mitophagy induction have previously demonstrated the recruitment of Atg8 to mitochondria; this allowed Atg8 interaction with Atg32, but whether Atg8 is already PE-lipidated when it is recruited to mitochondria is unknown (Kondo-Okamoto et al., 2012). Our observation showing that, in the Δ*psd1* strain, Atg8 fails to localize in mitochondria under nitrogen starvation, suggests that Psd1 could supply PE for Atg8 lipidation.

Our hypothesis concerning mitochondria as a source of PE and/or membranes is consistent with the observations of Hailey et al. in mammalian cells (Hailey et al., 2010). In their work, they showed that in starved NRK58B cells, the early autophagosomal marker Atg5 transiently localizes to puncta on mitochondria in the same way as do LC3 proteins (the Atg8 homologs), which identified mitochondria as membrane sources of starvation-induced autophagosomes. They showed that this autophagosome–mitochondria overlap during starvation is not due to mitophagy, and proposed that these contacts mediate the lipid transfer between both organelles. They also observed that autophagosome induction during starvation is inhibited severely when ER–mitochondria connections are impaired in cells. Moreover, these ER–mitochondria connections have also been shown to be important for mitophagy (Böckler and Westermann, 2014). In yeast, the ERMES complex, a protein

Journal of Cell Science (2019) 132, jcs221655. doi:10.1242/jcs.221655

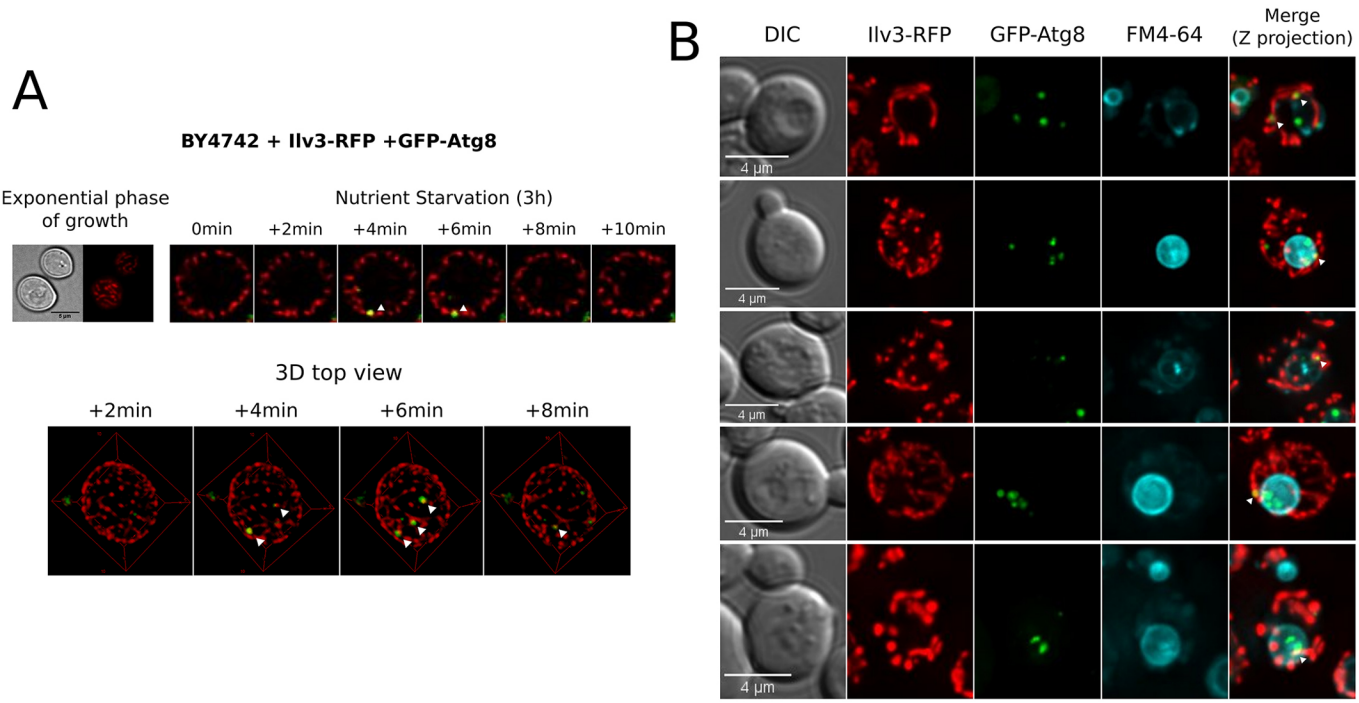

Fig. 7. Nitrogen starvation induces colocalization of GFP–Atg8 with mitochondria in close proximity to the vacuole. (A) BY4742 cells grown in a medium supplemented with a respiratory carbon source and expressing GFP–Atg8 and Ilv3–RFP were submitted for 1 h of nitrogen starvation. Then, cells were observed under a fluorescence videomicroscope for 2 h. Every 2 min, *Z*-stacks were recorded for each channel and images were deconvolved using the DeconvolutionLab plugin (Sage et al., 2017) for ImageJ. The lower row presents a 3D reconstruction of the upper images observed from the top. (B) BY4742 cells grown under the same conditions as described in A were submitted for 2 h of nitrogen starvation in the presence of FM4-64, a dye that allows visualization of the vacuoles, and observed under a fluorescence microscope as described in the Materials and Methods. *Z*-stacks of random planes were captured and each image channel was deconvolved as in A.

complex that links the ER with mitochondria and may have a role in promoting exchange of Ca^{2+} and phospholipids between the two organelles, is a major player contributing to mitophagy but not to autophagy. In ERMES mutants, colocalization between Atg8 and Atg32 is not affected; nevertheless, mitophagy is impaired (Böckler and Westermann, 2014). Consequently, this complex is hypothesized to facilitate exchange of lipids between ER and mitochondria and perhaps between ER and phagophores.

In our study, we highlighted a specific role of Psd1 in nitrogen starvation-induced mitophagy. We understand that the purpose of mitophagy induced during nitrogen starvation and the stationary phase of cell growth is most probably different (Fig. 8). When cells are grown under respiratory conditions that allow full differentiation of mitochondria and then are submitted to nitrogen starvation, they initiate degradation of some unnecessary mitochondria to provide nutrients required for their survival. On the other hand, the goal of mitophagy induced during the stationary phase of growth is to eliminate damaged mitochondria. This can be attested to by the increase in oxidized mitochondrial proteins in the Δ*atg32* strain, which is impaired in mitophagy (N.C., unpublished results). Moreover, we hypothesize that under nitrogen starvation, cells degrade mitochondria that are in close proximity to the vacuole preferentially, whereas in the stationary phase of growth, damaged mitochondria anywhere in the cell might be targeted for degradation (Fig. 8). We previously performed electron microscopy kinetics studies on the WT strain grown in respiratory conditions and submitted to nitrogen starvation. We observed two distinct waves of mitophagy. The first one took place in the first hours of nitrogen starvation, and we visualized contacts between the vacuole and mitochondria, followed by the appearance of vesicles containing mitochondria with only residual cytosol almost exclusively. The second wave appeared later, where vesicles containing mitochondria and significant amounts of cytosol were observed (Kiššová et al., 2007). The first event suggested a direct targeting of mitochondria for degradation, or 'micromitophagy', with a direct recruitment of autophagy machinery to mitochondria; the second wave suggested non-specific mitophagy. In the present study, we first confirmed GFP–Atg8 recruitment to mitochondria after 3 h of nitrogen starvation in WT cells by western immunodetection analyses (Fig. 4A) and immunoelectron microscopy (Fig. 5A). In Δ*psd1* cells, we observed a decrease of GFP–Atg8 localization to mitochondria in the same condition compared with WT, suggesting that Δ*psd1* mitophagy defect may be due to the failure to recruit Atg8 to mitochondria (Figs 4B and 5B). To test this hypothesis, we prepared purified mitochondrial extracts from our WT and Δ*psd1* cells, and tried to separate both Atg8 and Atg8-PE forms by western blot. Despite all our attempts, we did not manage to separate both Atg8 forms, but we confirmed the recruitment of two proteins of Atg8-conjugation machinery, Atg3 and Atg4, to mitochondria (Fig. 6A–C), suggesting that Atg8 is processed on mitochondria directly in response to nitrogen starvation. Then, to have a direct sequestration of mitochondria by the vacuole or micromitophagy, proximity between the PAS, the vacuole, and mitochondria seems necessary (Fig. 8). The findings that, during the first hours of nitrogen starvation, contacts between mitochondria and vacuoles occur and that some core autophagic proteins are recruited to mitochondria, as confirmed by fluorescence observations, support for this hypothesis (Fig. 7). At this point, we can hypothesize that Atg8 might be recruited and maintained on mitochondrial surface to be lipidated directly under nitrogen starvation, after which autophagy machinery might be

Journal of Cell Science (2019) 132, jcs221655. doi:10.1242/jcs.221655

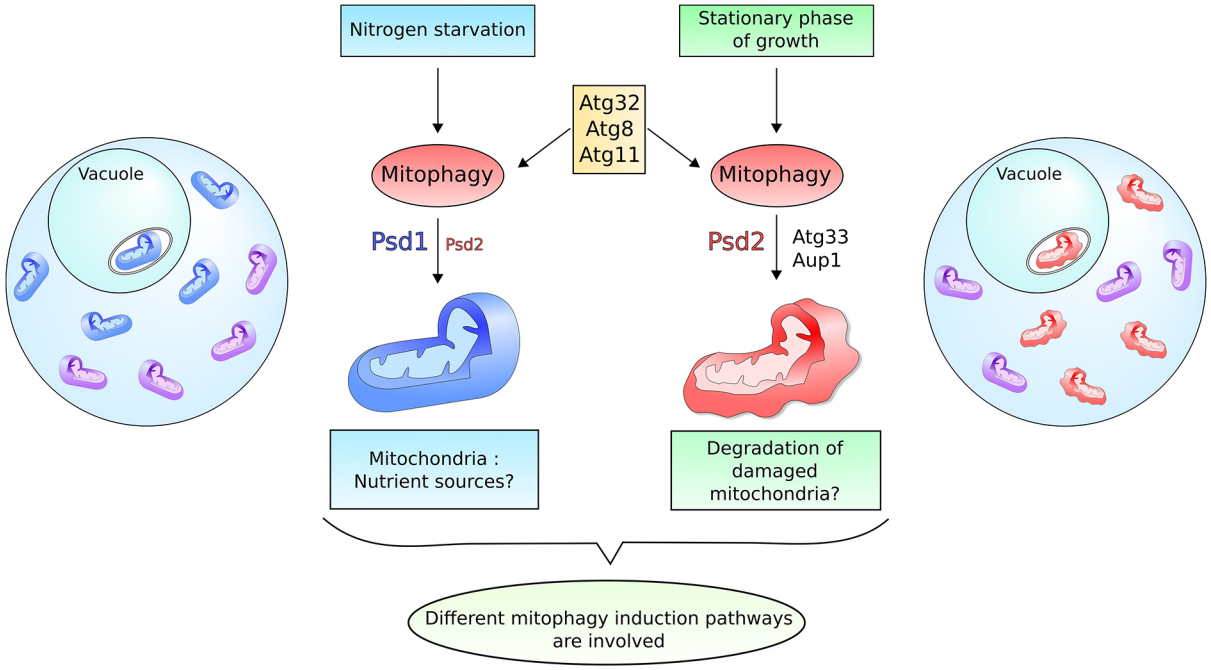

Fig. 8. Depending on the condition of induction, mitophagy may exploit different signaling pathways. Nitrogen starvation and the stationary phase of growth are two completely different mitophagy-inducing conditions. Under both conditions, the process requires the same key proteins such as Atg32, Atg11 and Atg8; however, the purpose of the process may differ. In nitrogen starvation, cells are harvested in a mid-exponential phase of growth and starved. Here, the majority of mitochondria are healthy/functional and mitophagy serves as sources of nutrients to ensure survival of cells under unfavorable conditions. In the stationary phase of growth, cells accumulate damaged components and mitophagy is useful to eliminate nonfunctional mitochondria. The fact, that Aup1 (Tal et al., 2007) and Atg33 (Kanki et al., 2009b) are only required for mitophagy in the stationary phase suggests that different signaling pathways are involved in mitophagy induction. We showed that Psd2, located in membranes of the vacuole, endosomes and Golgi, is the only protein involved in yeast PE synthesis that is required for mitophagy induced by the stationary phase of cell growth. Psd2 is also involved in nitrogen starvation-induced mitophagy, but its contribution is less important than of that of Psd1, the mitochondrial phosphatidylserine decarboxylase, which is selectively required for elimination of mitochondria under starvation.

recruited. In the absence of Psd1, Atg8 might fail to be retained to mitochondria and autophagy machinery might not be recruited to these organelles, leading to the mitophagy defect.

In yeast, Atg8 is encoded by one single gene and it is the only protein shown to be anchored to phagophore and autophagosome membranes. In mammalian cells, seven Atg8 homologs from different transcripts and genes have been characterized and are subdivided into two groups, LC3s (also known as MAP1LC3s) and GABARAPs (Schaaf et al., 2016). Because of strong sequence similarities, these proteins are believed to perform similar functions in autophagy; nevertheless, substantial evidence shows that the LC3/GABARAP family proteins are unique in function and important in autophagy-independent mechanisms (Schaaf et al., 2016). We can wonder whether each LC3 or GABARAP protein is lipidated with PE produced by different PE synthesis pathways in mammals depending on the mitophagy induction conditions. Our data in yeast highlight the role of phosphatidylserine decarboxylase (PSD) activity in mitophagy induction during the stationary phase of growth and in nitrogen starvation (Fig. 8). Therefore, it is possible that PSDs could have a central role in PE supplying for mitophagy in mammals. Our results are also in line with data showing that PE for Atg8 lipidation and membranes necessary for phagophore expansion are provided in different places in the cells depending on the purpose of autophagy or mitophagy.

MATERIALS AND METHODS

Yeast strains, plasmids and growth conditions

All yeast strains used in this study are listed in Table S1. BY4742 was used as wild-type (WT) strain. All strains were obtained from Euroscarf bank. Plasmids and gene deletion protocols are described below. Yeast cells were grown aerobically at 28°C in minimal medium (0.175% yeast nitrogen base without amino acids and ammonium sulfate, 0.5% ammonium sulfate, 0.1% potassium phosphate, 0.2% Drop-Mix, 0.01% of auxotrophic amino acids and nucleotide, pH 5.5), supplemented with 2% lactate as a carbon source. Cell growth was followed by measuring the optical density at 600 nm (OD_{600nm}). For starvation experiments, cells were harvested (5000 ***g*** for 5 min) at the early exponential phase of growth, washed three times with water and incubated in nitrogen starvation medium (0.175% yeast nitrogen base without amino acids and ammonium sulfate, and 2% lactate, pH 5.5). Autophagy was studied in cells expressing GFP–Atg8 after 6 h of nitrogen starvation or after 1 day of stationary phase growth (Noda et al., 1995). pRS416-*GFP-ATG8* was a gift from Dr Dan Klionsky (University of Michigan, Ann Arbor, MI). Mitophagy was studied in cells expressing Idp–GFP protein submitted to nitrogen starvation for 3 or 6 h or 1 day of stationary phase growth. The plasmid p*IDP1-GFP* was a gift from Dr Hagay Abeliovich (Hebrew University of Jerusalem, Jerusalem, Israel). BY4742 strains expressing Atg3–GFP or Atg4–GFP were a gift from Dr Isabelle Sagot (IBGC, Bordeaux, France). For PHO8 disruption, the *PHO8* gene was deleted in the BY4742 genetic background as follows: *PHO8* was amplified by PCR using the *PHO8* XmaI forward primer (5′-GCACCTGCAATCCCGGGAAA-TCTCAAC-3′) and the *PHO8* XmaI reverse primer (5′-CTTTAAGT-CCCGGGATCATTCTTTAAAG-3′) and cloned into XmaI-digested pFL39. Then, the *HIS3* gene was amplified by PCR using the *HIS3* StuI forward primer (5′-GATCCGCTGCACAG-GCCTGTTCCCTAGC-3′) and the *HIS3* ApaI reverse primer (5′-TACCACCAGAAGGGCCCTTAGATCTGC-3′) and cloned within *PHO8* gene in a StuI/ApaI-digested pFL39-*PHO8* plasmid. The *PHO8-HIS3* disruption fragment was amplified by PCR using the *PHO8-HIS3* forward primer (5′-GGGAAATCTCAACAGTCTCTTACTG-3′) and the *PHO8-HIS3* reverse primer (5′-CTTTAAAGAGGAAAAGGG-TACCTCC-3′), and BY4742 cells were transformed with *PHO8-HIS3* disruption fragment.

Journal of Cell Science (2019) 132, jcs221655. doi:10.1242/jcs.221655

For DPL1 disruption, the *DPL1* gene was deleted in the BY4742 genetic background following the same principle as for *PHO8* disruption. *DPL1* was amplified by PCR using the *DPL1* NotI forward primer (5′-ATATATACCGGGCGGCCGCATCGGG-3′) and the *DPL1* ApaI reverse primer (5′-CGTTCCTGTTCGGGCCCTTTAATA-3′), and cloned into NotI/ApaI–digested pRS314 plasmid. The *HIS3* gene was amplified by PCR using the *HIS3* XmaI forward primer (5′-GCAATTTCTAC-CCGGGTTCAGCAAC-3′) and the *HIS3* XmaI reverse primer (5′-GGCACTCCCGGGTTTTCCTCTTAAG-3′) and cloned within the *DPL1* gene in the pRS314-*DPL1* plasmid. Then, the *DPL1-HIS3* disruption fragment was amplified by PCR using the *DPL1-HIS3* forward primer (5′-ATTGGTATATTTTCAGTACAC-3′) and the DPL1-HIS3 reverse primer (5′-TTTAATAACTTGATGGCAATG-3′) and BY4742 cells were transformed with the *DPL1-HIS3* disruption fragment. For pESC-HIS3-PSD1 making, the *PSD1* gene was amplified by PCR using the *PSD1* NotI forward primer (5′-CAAAAAGAAGCGGCCGCCTTGGACTATAAG-3′) and the *PSD1* ClaI reverse primer (5′-CATTTTAAATCAATCGATCC-AATTATGCCTAATTTC-3′) and cloned in pESC-*HIS3* plasmid. For making pESC-HIS3-mtPSD2-V5, the mitochondrial-targeting sequence (MTS) of the *COXIV* gene was cloned into pESC-*HIS3* plasmid using the *COXIV-MTS* BamHI forward primer (5′-TCCCTGTCAGGATCCTTT-AGTCAA-3′) and the *COXIV-MTS* ApaI reverse primer (5′-ACGGG-TTGGGGCCCAAGCAGATAT-3′). Then, the *PSD2* gene was cloned upstream of the *COXIV-MTS* sequence in pESC-*HIS3* with the *COXIV-MTS-PSD2* ApaI forward primer (5′-TGGTAAAGAATCCTCGATTT-TCAGGAGCATCCAACGACGGGGCCCAGGATTATTAAGGGCAGA-AAGCGAG GCAAGAACAAGAAG-3′) and the *COXIV-MTS-PSD2* XhoI reverse primer containing the V5 tag sequence (5′-GCTTCACTCGAGC-GTAGAATCGAGACCGAGGAGAGGGTTAGGGATAGGCTTACCTTC-GAAGGGTAGCCCAGCAAAATCTTTAT-3′). For making pESC-HIS3-PSD2-V5, the *PSD2* gene was cloned into pESC-*HIS3* using the *PSD2-V5* ApaI forward primer (5′-TGGTAAAGAATCCTCGATTTTCAGGAGG-GGCCCACGACGAAGATGAGGATTATTAAGGGCAGAAAGCGAGG-CAAGAACAAG-3′) and the *COXIV-MTS-PSD2* XhoI reverse primer containing V5-tag sequence (5′-GCTTCACTCGAGCGTAGAATCGA-GACCGAGGAGAGGGTTAGGGATAGGCTTACCTTCGAAGGGTAG-CCCAGCAAAATCTTTAT-3′).

Preparation of protein extracts and western blotting

For preparation of total protein extract, 2×10^7 cells were harvested by centrifugation, washed with water and resuspended in 450 µl of water and 50 µl of lysis buffer (1.85 M NaOH, 3.5% β-mercaptoethanol). After 10 min on ice, 50 µl of 3 M trichloroacetic acid was added followed by another incubation of 10 min on ice. Proteins were pelleted by centrifugation (13,000 ***g*** for 8 min), washed with acetone and resuspended in 20 µl of 5% SDS and 20 µl of loading buffer (2% β-mercaptoethanol, 2% SDS, 0.1 M Tris-HCl pH 8.8, 20% glycerol, 0.02% Bromophenol Blue). Samples were boiled for 5 min and 50 µg of proteins were separated by electrophoresis on 12.5% SDS-PAGE gels and subjected to immunoanalysis with either anti-GFP antibody (1:5000, cat no. 11844460001; Roche), anti-Pgk1 antibody (1:5000, cat no. 459250; Invitrogen) or anti-porin antibody (1:5000, cat no. 459500; Invitrogen). Detection was performed with ECL$^+$ reagent (Perkin Elmer) and western blot quantifications were undertaken using ImageJ Software (NIH). For preparation of cell lysates, 5×10^7 cells were broken with glass beads in buffer containing 0.6 M mannitol, 5 mM MES pH 6; lysates were centrifuged for 10 min at 800 ***g***. The supernatants were loaded on 10–60% OptiPrep™ density gradients in buffer with 5 mM MES pH6, 5 mM EDTA, 10 mM NEM plus protease inhibitor cocktail (Roche).

ALP activity

Alkaline phosphatase activity was measured on various Δ*pho8* strains expressing the mitochondrial-targeted truncated version of Pho8, mtPho8Δ60, during the exponential phase of growth or after 6 h of nitrogen starvation. For each point, five OD_{600nm} of cells expressing mitochondrial-targeted Pho8Δ60 (mtPho8Δ60) were harvested and lysed with glass beads into lysis buffer (20 mM PIPES, 0.5% Triton X-100, 50 mM KCl, 100 mM potassium acetate, 10 mM $MgCl_2$, 10 µM $ZnSO_4$ and 2 mM PMSF). After centrifugation (800 ***g*** for 15 min), 20 µl of supernatant was put with 80 µl of water and 400 µl of activity buffer (250 mM Tris-HCl pH 8, 0.4% Triton X-100, 10 mM $MgCl_2$, 10 µM $ZnSO_4$, 125 mM p-nitrophenyl-phosphate) for 20 min at 30°C. The reaction was stopped by the addition of 500 µl of 1 M glycine pH 11. Activity was then measured by determining the optical density at 400 nm. Protein concentration was measured with the Lowry method (Lowry et al., 1951). ALP activities are expressed as arbitrary fluorescence units/min/mg protein (AU/min/mg).

Mitochondria purification and density gradient centrifugation analysis

Cells were harvested (5000 ***g*** for 5 min) and washed three times with water and incubated for 15 min at 28°C in a pre-incubating buffer (0.5 M β-mercaptoethanol, 0.1 M Tris-HCl pH 9.3). After three washes with Tris-HCl KCl buffer (10 mM Tris-HCl pH 7, 0.5 M KCl), cells were digested in digestion buffer (1.35 M sorbitol, 10 mM citric acid, 30 mM Na_2HPO_4, 1 mM EGTA, zymolyase 20T at 20 mg/g of dry weight). Spheroplasts were washed twice in isotonic buffer [0.75 M sorbitol, 0.4 M mannitol, 10 mM Tris-maleate, 0.1% bovine serum albumin (BSA), pH 6.8] and resuspended in homogenization buffer (0.6 M mannitol, 10 mM, Tris-maleate, 2 mM EGTA, 0.2% BSA, pH 6.8). Spheroplasts were broken using a blender. Unbroken spheroplasts and heavy cell compartments were pelleted by centrifugation at 700 ***g*** for 10 min, and the supernatant was centrifuged for 10 min at 12,000 ***g***. The pellet was resuspended in the final buffer (0.6 M mannitol, 2 mM EGTA, 10 mM Tris-maleate, pH 6.8), centrifuged at 700 ***g*** for 10 min, and the supernatant was centrifuged at 12,000 ***g*** for 10 min to pellet mitochondria. Then crude mitochondrial extract was resuspended in the final buffer with anti-proteases (Roche, cat no. 11836170001) and 1 mg of proteins were loaded on a 20–60% continuous sucrose gradient and centrifuged overnight at 134,000 ***g***. Then fractions were collected and analyzed by western immunodetection analyses using anti-GFP antibody, anti-porin antibody, anti-Pgk1 antibody (all as above), anti-Dpm1 antibody (1:5000, cat no. A6429; Life Technologies).

Mitochondria fractionation

500 µg of mitochondria were resuspended and incubated in 100 µl of cold 0.1 M Na_2CO_3 (pH 11.0) or 0.1% TX-100 for 30 min in ice. The suspensions were ultra-centrifuged at 4°C for 15 min at 90,000 ***g***. Then, supernatants and pellets were incubated in 500 µl of 12.5% trichloroacetic acid for at least 15 min in ice, followed by centrifugation for 15 min at 20,000 ***g*** at 4°C. The samples were washed with 500 µl of acetone and dried for 5 min at room temperature. Then, the pellet was resuspended in 40 µl of Laemmli buffer and analyzed by SDS-PAGE.

Lipid extraction

To extract lipids from isolated mitochondria, 2 ml of chloroform:methanol (2:1, v/v) was added to 500 µg of mitochondria. Following vigorous shaking and centrifugation, the organic phase was put aside, and the aqueous phase was washed again with 2 ml of chloroform. The combined organic phases containing lipids were dried and redissolved in 200 µl chloroform:methanol (2:1, v/v) and 800 µl of ether solution. The suspension was incubated 1 h at −20°C and dried. Next, extracts were resuspended in 30 µl MeOH-$HCCl_3$ (1:2, v/v) and the lipids were separated by one-dimensional high-performance thin-layer chromatography (TLC) using 20×20 cm TLC plates. Migration buffer was prepared as follows: chloroform:methanol:1-propanol:methyl acetate:0.25% aqueous KCl (28:10:25:25:7, v/v/v/v/v). Then, the plates were dried and lipids were visualized with 8% phosphoric acid in 3% copper acetate buffer. Lipid identity was based on the mobility of known standards. Quantification was performed with ImageJ.

Fluorescence microscopy

Video microscopy on cells expressing Ilv3–dsRed and GFP–Atg8 proteins was carried out with Leica DMI6000B Video-spinning-disk-FRAP microscope with Photometrics Quantem 512 EMCCD camera. For vacuole staining, cells were incubated for 1 h with 40 µM FM4-64 and observed with a Leica DMI8 Video-microscope equipped with a large field, highly sensitive ORCA-Flash 4.0 v2 digital CMOS camera from Hamamastu. Microscopes are located in the Bordeaux Imaging Center

(BIC). Images were deconvoled using a DeconvolutionLab plugin developed for ImageJ software (NIH) (Sage et al., 2017).

Electron microscopy and immunoelectron microscopy

For electron microscopy experiments, cells were grown in the presence of 1 mM PMSF. Harvested cells were placed on the surface of formvar-coated copper grids (400 mesh). Each loop was quickly submersed in liquid propane (−180°C) and transferred to a precooled solution of 4% osmium tetroxide in dry acetone at −82°C for 48 h for substitution/fixation. Samples were gradually warmed to room temperature, and washed in dry acetone. Specimens were stained for 1 h with 1% uranyl acetate in acetone at 4°C, rinsed and infiltrated with araldite (epoxy resin, Fluka; ref. 10951-1L). Ultra-thin sections were stained with lead citrate. Observations were performed on a Philips Tecnai 12 Biotwin (120 kV) electron microscope.

For immunoelectron microscopy, the loops were transferred into a precooled solution of 0.1% glutaraldehyde in dry acetone for 3 days at −82°C. Samples were rinsed with acetone at −20°C, and embedded progressively at −20°C in LR Gold resin (EMS, USA). Resin polymerization was carried out at −20°C for 7 days under UV illumination. Ultrathin LR Gold sections were collected on nickel grids coated with formvar. Sections were first incubated for 5 min with 1 mg/ml glycine, and for 5 min with fetal calf serum (1:20). The grids were incubated 45 min at room temperature with goat anti-Atg8 monoclonal antibody (1:100, cat. no. Sc15639, Molecular Probes) rinsed with Tris-buffered saline (TBS) containing 0.1% BSA and then incubated for 45 min at room temperature with anti-mouse- or anti-rabbit IgG conjugated to 10 nm gold particles (BioCell). The sections were rinsed with distilled water, and contrasted through a 5 min incubation with 2% uranyl acetate in water, followed by 1 min incubation with 1% lead citrate. Observations were performed on a Philips Tecnai 12 Biotwin (120 kV) electron microscope.

Statistical analysis

P-values were calculated using unpaired Student's *t*-tests; $P<0.05$ was considered statistically significant.

Acknowledgments

We thank Drs Sagot, Klionsky and Abeliovich for the gift of strains and material, Fabrice Cordelières for his help with deconvolution and fluorescence image analyses, and Eric Testet and Amélie Bernard for technical help and fruitful discussion.

Competing interests

The authors declare no competing or financial interests.

Author contributions

Methodology: N.C.; Validation: N.C.; Investigation: P.V., E.C., B.S., C.B., N.C.; Writing - original draft: N.C.; Writing - review & editing: P.V., I.B.-K., N.C.; Visualization: P.V.; Supervision: I.B.-K., N.C.

Funding

The work in the laboratories of the authors was supported by grants from the Slovak Academic Information Agency (SK-FR-2015-0005) (to I.B.-K.), the Centre National de la Recherche Scientifique (CNRS), the Université de Bordeaux and the Doctoral International Program from IDEX of Bordeaux supported by Agence Nationale pour la Recherche (ANR-10-IDEX-03-02) (to N.C. and P.V.). The France–Slovakia collaboration was supported by Campus France (Stefanik no. 35809VC) (to N.C. and I.B.-K.).

Supplementary information

Supplementary information available online at
http://jcs.biologists.org/lookup/doi/10.1242/jcs.221655.supplemental

References

Axe, E. L., Walker, S. A., Manifava, M., Chandra, P., Roderick, H. L., Habermann, A., Griffiths, G. and Ktistakis, N. T. (2008). Autophagosome formation from membrane compartments enriched in phosphatidylinositol 3-phosphate and dynamically connected to the endoplasmic reticulum. *J. Cell. Biol.* **182**, 685-701.

Bhatia-Kiššová, I. and Camougrand, N. (2010). Mitophagy in yeast: actors and physiological roles. *FEMS Yeast Res.* **10**, 1023-1034.

Birner, R., Bürgermeister, M., Schneiter, R. and Daum, G. (2001). Roles of phosphatidylethanolamine and of its several biosynthetic pathways in *Saccharomyces cerevisiae*. *Mol. Biol. Cell.* **12**, 997-1007.

Böckler, S. and Westermann, B. (2014). Mitochondrial ER contacts are crucial for mitophagy in yeast. *Dev. Cell.* **28**, 450-458.

Bürgermeister, M., Birner-Grünberger, R., Heyn, M. and Daum, G. (2004). Contribution of different biosynthetic pathways to species selectively of aminoglycerophopholipids assembled into mitochondrial membranes of the yeast *Saccharomyces cerevisiae*. *Biochim. Biophys. Acta* **1686**, 148-160.

Calzada, E., Onguka, O. and Claypool, S. M. (2016). Phosphatidylethanolamine metabolisme in Health and Disease. *Int. Rev. Cell Mol. Biol.* **321**, 29-88.

Choi, A. M. K., Ryter, S. W. and Levine, B. (2013). Autophagy in human health and disease. *N. Engl. J. Med.* **368**, 651-662.

Daum, G. and Vance, J. E. (1997). Import of lipids into mitochondria. *Prog. Lipid Res.* **36**, 103-130.

Feng, Y., He, D., Yao, Z. and Klionsky, D. J. (2014). The machinery of macroautophagy. *Cell. Res.* **24**, 24-41.

Friedman, J. R., Kannan, M., Toulmay, A., Jan, C. H., Weissman, J. S., Prinz, W. A. and Nunnari, J. (2018). Lipid homeostasis is maintained by dual targeting of the mitochondrial PE biosynthesis enzyme to the ER. *Dev. Cell* **44**, 261-270.

Gulshan, K., Shahi, P. and Moye-Rowley, W. S. (2010). Compartment-specific synthesis of phosphatidylethanolamine is required for normal heavy metal resistance. *Mol. Biol. Cell.* **21**, 443-455.

Hailey, D. W., Rambold, A. S., Satpute-Krishnan, P., Mitra, K., Sougrat, R., Kim, P. K. and Lippincott-Schwartz, J. (2010). Mitochondria supply membranes for autophagosome biogenesis during starvation. *Cell* **141**, 656-667.

Horvath, S. E., Wagner, A., Steyer, E. and Daum, G. (2011). Metabolic link between phosphatidylethanolamine and triacylglycerol metabolism in the yeast *Saccharomyces cerevisiae*. *Biochem. Biophys. Acta.* **1811**, 1030-1037.

Ichimura, Y., Kirisako, T., Takao, T., Satomi, Y., Shimonishi, Y., Ishihara, N., Mizushima, N., Tanida, I., Kominami, E., Ohsumi, M. et al. (2000). A ubiquitin-like system mediates protein lipidation. *Nature* **408**, 488-492.

Jacob, J. A., Salmani, J. M. M., Jiang, Z., Feng, L., Song, J., Jia, X. and Chen, B. (2017). Autophagy: an overview and its roles in cancer and obesity. *Clinica Chemica acta.* **468**, 85-89.

Kanki, T. and Klionsky, D. J. (2008). Mitophagy in yeast occurs through a selective mechanism. *J. Biol. Chem.* **283**, 32386-32393.

Kanki, T., Wang, K., Cao, Y., Baba, M. and Klionsky, D. J. (2009a). Atg32 is a mitochondrial protein that confers selectivity during mitophagy. *Dev. Cell.* **17**, 98-109.

Kanki, T., Wang, K., Baba, M., Bartholomew, C. R., Lynch-Day, M. A., Du, Z. Geng, J., Mao, K., Yang, Z. and Klionsky, D. J. (2009b). A genomic screen for yeast mutants defective in selective mitochondria autophagy. *Mol. Biol. Cell.* **20**, 4730-4738.

Kirisako, T., Ichimura, Y., Okada, H., Kabeya, Y., Mizushima, N., Yoshimori, T., Ohsumi, M., Takao, T., Noda, T. and Ohsumi, Y. (2000). The reversible modification regulates the membrane-binding state of Apg8/Aut7 essential for autophagy and the cytoplasm to vacuole targeting pathway. *J. Cell. Biol.* **151**, 263-276.

Kissová, I., Deffieu, M., Manon, S. and Camougrand, N. (2004). Uth1p is involved in the autophagic degradation of mitochondria. *J. Biol. Chem.* **279**, 39068-39074.

Kiššová, I., Salin, B., Schaeffer, J., Bhatia, S., Manon, S. and Camougrand, N. (2007). Selective and non-selective autophagic degradation of mitochondria in yeast. *Autophagy* **3**, 329-336.

Klug, L. and Daum, G. (2014). Yeast lipid metabolism at a glance. *FEMS Yeast Res.* **14**, 369-388.

Kondo-Okamoto, N., Noda, N. N., Suzuki, S. W., Nakatogawa, H., Takahashi, I., Matsunami, M., Hashimoto, A., Inagaki, F., Ohsumi, Y. and Okamoto, K. (2012). Autophagy-related protein 32 acts as autophagic degron and directly initiates mitophagy. *J. Biol. Chem.* **287**, 10631-10638.

Lowry, O. H., Rosebrough, N. J., Farr, A. L. and Randall, R. J. (1951). Protein measurement with the Folin phenol reagent. *J. Biol. Chem.* **193**, 265-275.

Mao, K., Wang, K., Zhao, M., Xu, T. and Klionsky, D. J. (2011). Two MAPK-signaling pathways are required for mitophagy in *Saccharomyces cerevisiae*. *J. Cell. Biol.* **193**, 755-767.

Mendl, N., Occhipinti, A., Müller, M. Wild, P., Dikic, I. and Reichert, A. S. (2011). Mitophagy in yeast is independent of mitochondrial fission and requires the stress response gene WHI2. *J. Cell Sci.* **124**, 1339-1350.

Mizushima, N., Noda, T., Yoshimori, T., Tanaka, Y., Ishii, T., George, M. D., Klionsky, D. J., Ohsumi, M. and Ohsumi, Y. (1998). A protein conjugation system essential for autophagy. *Nature* **395**, 395-398.

Nebauer, R., Rosenberger, S. and Daum, G. (2007). Phosphatidylethanolamine, a limiting factor of autophagy in yeast strains bearing a defect in the carboxypeptidase Y pathway of vacuolar targeting. *J. Biol. Chem.* **282**, 16736-16743.

Noda, T., Matsuura, A., Wada, Y. and Ohsumi, Y. (1995). Novel system for monitoring autophagy in the yeast *Saccharomyces cerevisiae*. *Biochem. Biophys. Res. Commun.* **210**, 126-132.

Okamoto, K., Kondo-Okamoto, N. and Ohsumi, Y. (2009). Mitochondria-anchored receptor Atg32 mediates degradation of mitochondria via selective autophagy. *Dev. Cell.* **17**, 87-97.

Ravikumar, B., Moreau, K., Jahreiss, L., Puri, C. and Rubinsztein, D. C. (2010). Plasma membrane contributes to the formation of pre-autophagosomal structures. *Nat. Cell Biol.* **12**, 747-757.

Riekhof, W. R., Wu, W.-I., Jones, J. L., Nikrad, M., Chan, M. M., Loewen, C. J. R. and Voelker, D. R. (2014). An assembly of proteins and lipid domains regulates transport of phosphatidylserine to phosphatidylserine decarboxylase 2 in *Saccharomyces cerevisiae*. *J. Biol. Chem.* **289**, 5809-5819.

Rockenfeller, P., Koska, M., Pietrocola, F., Minois, N., Knittelfelder, O., Sica, V., Franz, J., Carmona-Gutierrez, D., Kroemer, G. and Madeo, F. (2015). Phosphatidylethanolamine positively regulates autophagy and longevity. *Cell Death Differ.* **22**, 499-508.

Sage, D., Donati, L., Soulez, F., Fortun, D., Schmit, G., Seitz, A., Guiet, R., Vonesch, C. and Unser, M. (2017). DeconvolutionLab2: an open-source software for deconvolution microscopy. *Methods* **115**, 28-41.

Schaaf, M. B. E., Keulers, T. G., Vooijs, M. A. and Rouschop, K. M. (2016). LC3/GABARAP family proteins: autophagy-(un)related functions. *FASEB J.* **30**, 3961-3978.

Schlumpberger, M., Schaeffeler, E., Straub, M., Bredschneider, M., Wolf, D. H. and Thumm, M. (1997). AUT1, a gene essential for autophagy in the yeast *Saccharomyces cerevisiae*. *J. Bacteriol.* **179**, 1068-1076.

Storey, M. K., Clay, K. L., Kutateladze, T., Murphy, R. C., Overduin, M. and Voelker, D. R. (2001). Phosphatidylethanolamine has an essential role in *Saccharomyces cerevisiae* that is independent of its ability to form hexagonal phase structures. *J. Biol. Chem.* **276**, 48539-48548.

Suzuki, K. (2013). Selective autophagy in budding yeast. *Cell Death Differ.* **20**, 43-48.

Tal, R., Winter, G., Ecker, N., Klionsky, D. J. and Abeliovich, H. (2007). Aup1p, a yeast mitochondrial protein phosphatase homolog, is required for efficient stationary phase mitophagy and cell survival. *J. Biol. Chem.* **282**, 5617-5624.

Tasset, I. and Cuervo, A. M. (2016). Role of chaperone-mediated autophagy in metabolism. *FEBS J.* **283**, 2403-2413.

Trotter, P. J. and Woelker, D. R. (1995). Identification of a non-mitochondrial phosphatidylserine decarboxylase activity (PSD2) in the yeast *Saccharomyces cerevisiae*. *J. Biol. Chem.* **270**, 6062-6070.

Trotter, P. J., Pedretti, J. and Voelker, D. R. (1993). Phosphatidylserine decarboxylase from *Saccharomyces cerevisiae*. Isolation of mutants, cloning of the gene, and creation of a null allele. *J. Biol. Chem.* **268**, 21416-21424.

Van der Vaart, A., Griffith, J. and Reggiori, F. (2010). Exit from the Golgi is required for the expansion of the autophagosomal phagophore in yeast *Saccharomyces cerevisiae*. *Mol. Biol. Cell.* **21**, 2270-2284.

Wen, X. and Klionsky, D. J. (2016). An overview of macroautophagy in yeast. *J. Mol. Biol.* **428**, 1681-1699.

Wilson-Zbinden, C., dos Santos, A. X., Stoffel-Studer, I., van der Vaart, A., Hofmann, K., Reggiori, F., Riezman, H., Kraft, C. and Peter, M. (2015). Autophagy competes for a common phosphatidylethanolamine pool with major cellular PE-consuming pathways in *Saccharomyces cerevisiae*. *Genetics* **199**, 475-485.

Zelinski, T. A. and Choy, P. C. (1982). Phosphatidylethanolamine biosynthesis in isolated hamster heart. *Can. J. Biochem.* **60**, 817-823.

Zinser, E., Sperka-Gottlieb, C. D., Fasch, E. V., Kohlwein, S. D., Paltauf, F. and Daum, G. (1991). Phospholipid synthesis and lipid composition of subcellular membranes in the unicellular eukaryote *Saccharomyces cerevisiae*. *J. Bacteriol* **173**, 2026-2034.

Table S1: Reagents and strains REAGENT

Antibodies	Source	Identifier
Mouse monoclonal Pgk1	Thermofisher	**Cat #** 459250
Mouse monoclonal Porin	Thermofisher	**Cat# 459500, RRID:AB_2532239**
Goat polyclonal Atg8	Santa Cruz	**Cat# sc-15639, RRID:AB_633983**
Mouse monoclonal V5	Thermofisher	**Cat#14-6796-80, RRID:AB_10717814)**
Mouse monoclonal GFP	ROCHE	**Cat# 11814460001, RRID:AB_390913**

STRAINS

Souche	**Génotype**
BY4742 (WT)	MATα; *his3Δ1*; *leu2Δ0*; *lys2Δ0*; *ura3Δ0*
BY + GFP-Atg8	BY4742 *pRS416-GFP-ATG8*
BY + Idp1-GFP	BY4742 p*IDP1-GFP*
Δ*psd1* + GFP-Atg8	BY4742 *psd1*::*kanMX4* pRS416-*GFP-ATG8*
Δ*psd1* + Idp1-GFP	BY4742 *psd1*::*kanMX4* p*IDP1-GFP*
Δ*psd1* + Idp1-GFP + p*PSD1*	BY4742 *psd1*::*kanMX4* p*IDP1-GFP* pRS416-*PSD1*
Δ*psd2* + GFP-Atg8	BY4742 *psd2*::*kanMX4* pRS416-*GFP-ATG8*
Δ*psd2* + Idp1-GFP	BY4742 *psd2*::*kanMX4* p*IDP1-GFP*
Δ*ept1* + GFP-Atg8	BY4742 *ept1*::*kanMX4* pRS416-*GFP-ATG8*
Δ*ept1* + Idp1-GFP	BY4742 *ept1*::*kanMX4* p*IDP1-GFP*
Δ*ale1* + GFP-Atg8	BY4742 *ale1*::*kanMX4* pRS416-*GFP-ATG8*
Δ*ale1* + Idp1-GFP	BY4742 *ale1*::*kanMX4* p*IDP1-GFP*
Δ*tgl3* + GFP-Atg8	BY4742 *tgl3*::*kanMX4* pRS416-*GFP-ATG8*
Δ*tgl3* + Idp1-GFP	BY4742 *tgl3*::*kanMX4* p*IDP1-GFP*
Δ*dpl1* + GFP-Atg8	BY4742 *dpl1*::*HIS3* pRS416-*GFP-ATG8*
Δ*dpl1* + Idp1-GFP	BY4742 *dpl1*::*HIS3* p*IDP1-GFP*
Δ*pho8* +mtPho8	BY4742 *pho8*::*kanMX4* + pFL39-*COXIV-PHO8Δ60*
Δ*psd1*Δ*pho8* +mtPho8	BY4742 *psd1*::*kanMX4 pho8::HIS3* pFL39-*COXIV-PHO8Δ60*
Δ*atg32*Δ*pho8* +mtPho8	BY4742 *atg32*::*kanMX4 pho8::HIS3* pFL39-*COXIV-PHO8Δ60*
Δ*psd1* + mtPsd2-V5 + Idp1-GFP	BY4742 *psd1*::*kanMX4 pho8::HIS3* pESC-*HIS3-COXIVmts-PSD2-V5* p*IDP1-GFP*
BY4742 + Atg3-GFP	BY4742 *atg3*::*ATG3-GFP*

BY4742 + Atg4-GFP	BY4742 *atg4*::*ATG4-GFP*
BY4742 + Atg32-V5	BY4742 pYES-*ATG32-V5*
Δ*psd1* + Atg32-V5	BY4742 *psd1*::*kanMX4* pYES-*ATG32-V5*
BY4742 + Ilv3-RFP + GFP-Atg8	*BY4742 pRS416-GFP-ATG8 pIlv3-GFP*

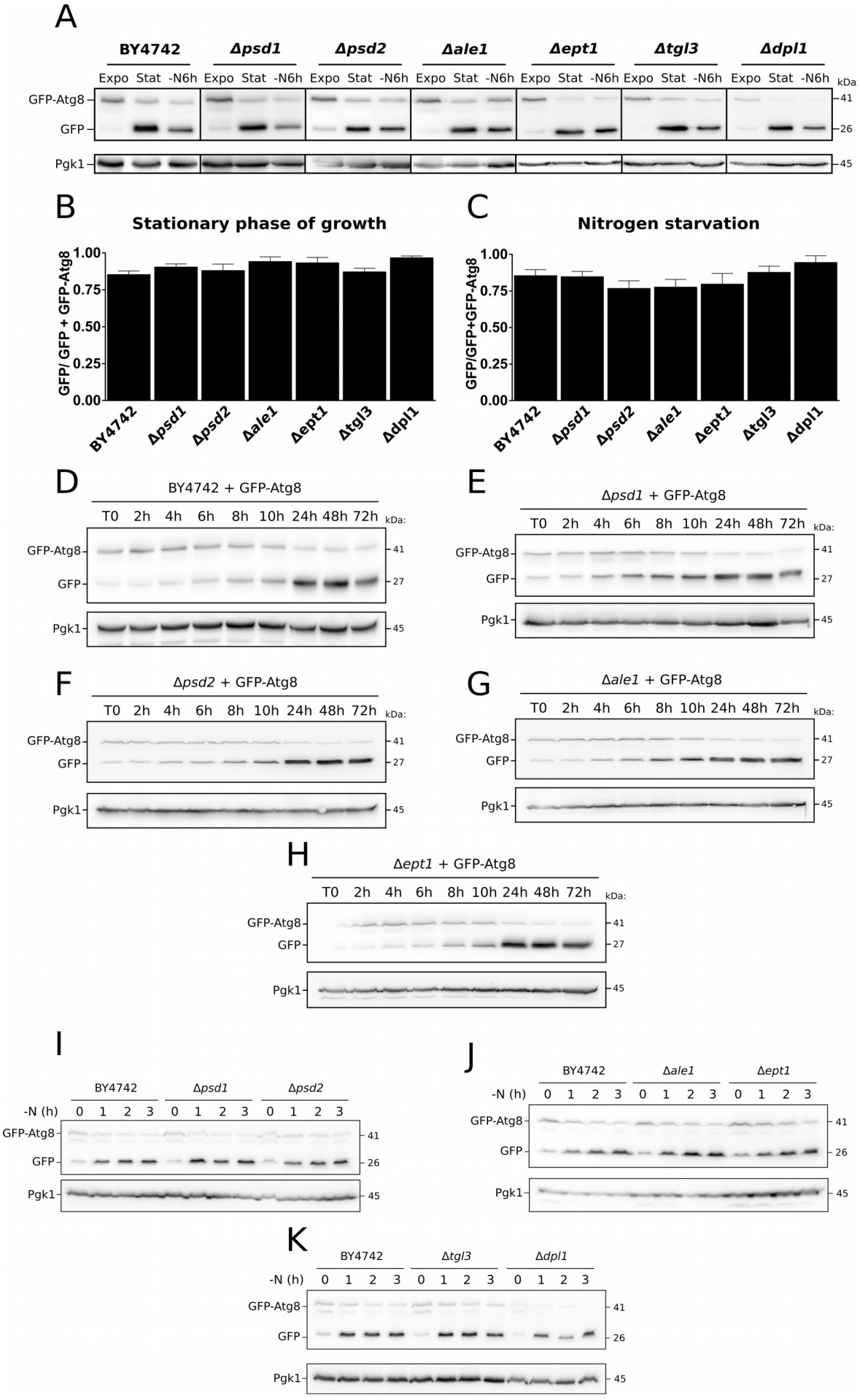

Figure S1: Autophagy induction is not altered in strains in which a single phosphatidylethanolamine pathway is impaired. (**A**) BY4742, *Δpsd1*, *Δpsd2*, *Δale1*, *Δept1*, *Δtgl3*, and *Δdpl1* strains grown in a respiratory carbon source medium and expressing GFP-Atg8, were harvested in a mid-exponential phase of growth (Expo) and submitted either for 6 hours of nitrogen starvation (-N6h) or 1 day of stationary phase of growth (Stat). Total protein extracts were prepared, separated in SDS PAGE and analyzed by western blots. For immunodetection, anti-GFP antibody was used to detect GFP-Atg8 and residual GFP. The cytosolic phosphoglycerate kinase, Pgk1, was used as loading control. Autophagy induction was quantified by calculating GFP/(GFP+GFP-Atg8) ratio in stationary phase of growth (**B**) or nitrogen starvation (**C**). Data were obtained from five independent experiments. BY4742 WT (**D**), *Δpsd1* (**E**), *Δpsd2* (**F**), *Δale1* (**G**) and *Δept1* (**H**) strains expressing GFP-Atg8, were harvested in a mid-exponential phase of growth (T0) and at the different time points until 72h after T0. Then, total protein extracts were prepared, proteins were separated by SDS-PAGE and GFP protein was visualized by western blots using Roche anti-GFP antibody. Pgk1, the cytosolic phosphoglycerate kinase was used as loading control. Experiments were performed twice with the same outcome. The same experiment was performed twice on cells used in (D-H) submitted for 1h, 2h or 3h of nitrogen starvation (**I**, **J**, **K**).

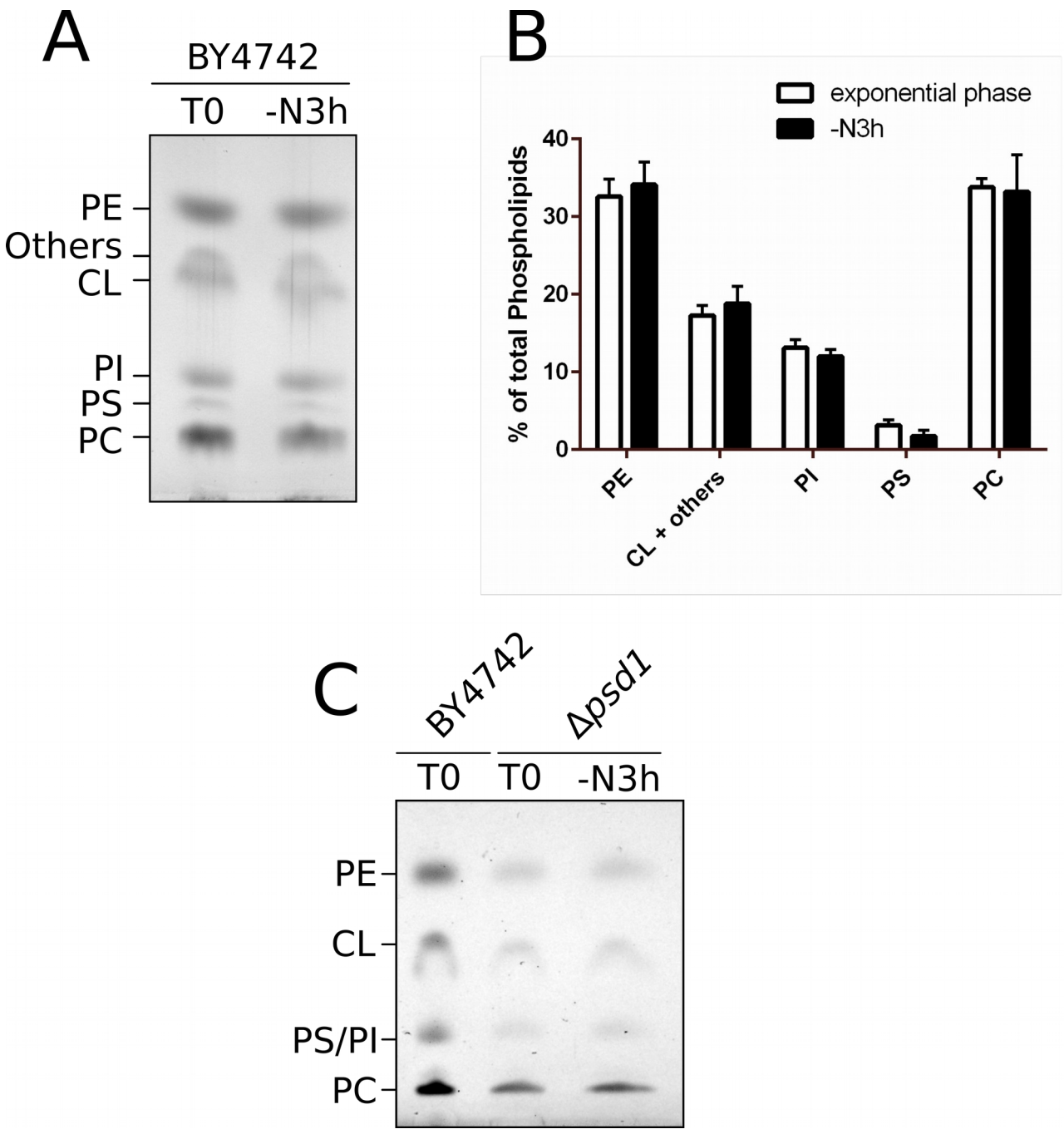

Figure S2: Nitrogen starvation does not affect lipid composition of mitochondria. (**A**) Mitochondria lipids were isolated from BY4742 cells harvested either in a mid-exponential phase of growth or after 3 hours of nitrogen starvation, separated by TLC afterward as described in the Material and Methods. (**B**) Lipids were quantified from TLC plates using ImageJ software (NIH). (**C**) The same experiment as described in (A) was carried out with mitochondria purified from Δ*psd1* cells, harvested in a mid-exponential phase of growth or after 3 hours of nitrogen starvation.

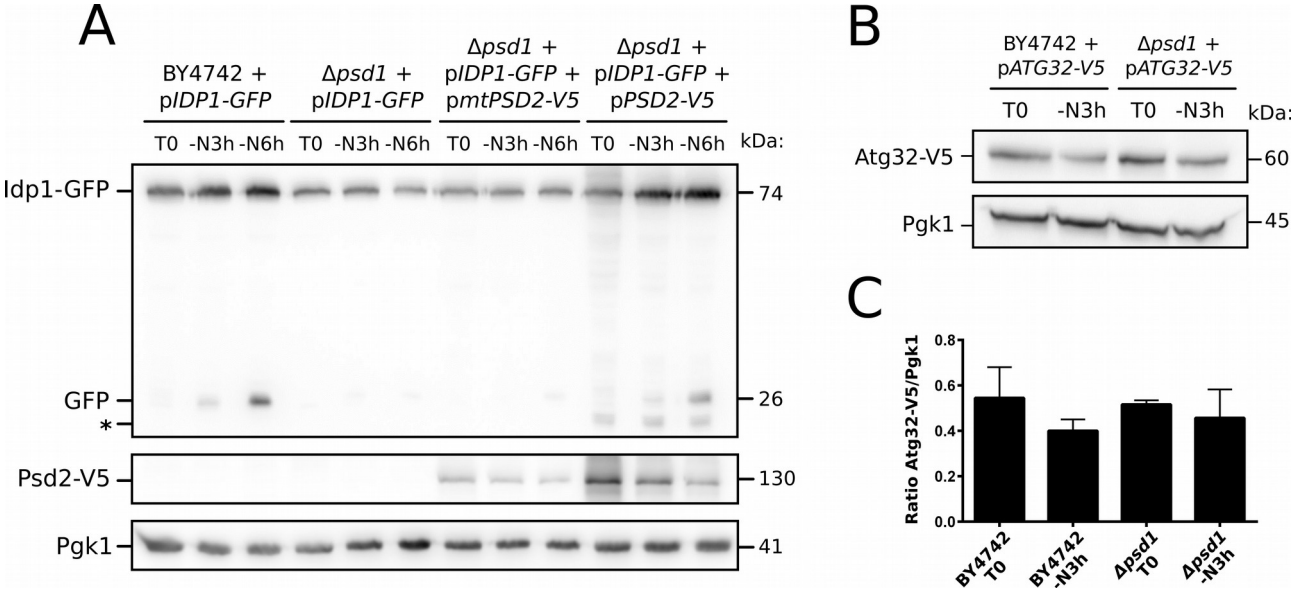

Figure S3: Overexpression of Psd2 rescues mitophagy defect in *Δpsd1* cells under nitrogen starvation. (**A**) Mitophagy was assessed using Idp1-GFP tool in *Δpsd1* cells overexpressing Psd2-V5 or a mitochondria-targeted version of Psd2-V5 (mtPSD2-V5). Cells were harvested in an exponential phase of growth (T0) or after 3 hours (-N3h) or 6 hours (-N6h) of nitrogen starvation, respectively. The corresponding total protein extracts were separated by SDS PAGE and analyzed by western-blots using anti-GFP antibody and anti-V5 antibody. Pgk1, the cytosolic phosphoglycerate kinase, was used as loading control. Results were obtained from 3 independent experiments. (**B**) Lactate-grown cells expressing Atg32-V5 were harvested either in an exponential phase of growth (T0) or after 3 hours of nitrogen starvation (-N3h). Then, total protein extracts were prepared, separated in SDS-PAGE and analyzed by western-blots. Anti-V5 antibody was used to detect Atg32-V5 protein. Pgk1, the cytosolic phosphoglycerate kinase, was used as loading control. (**C**) The ratio Atg32-V5/Pgk1 was calculated to appreciate Atg32-V5 expression in the corresponding strains and conditions. Results were obtained from three independent experiments.

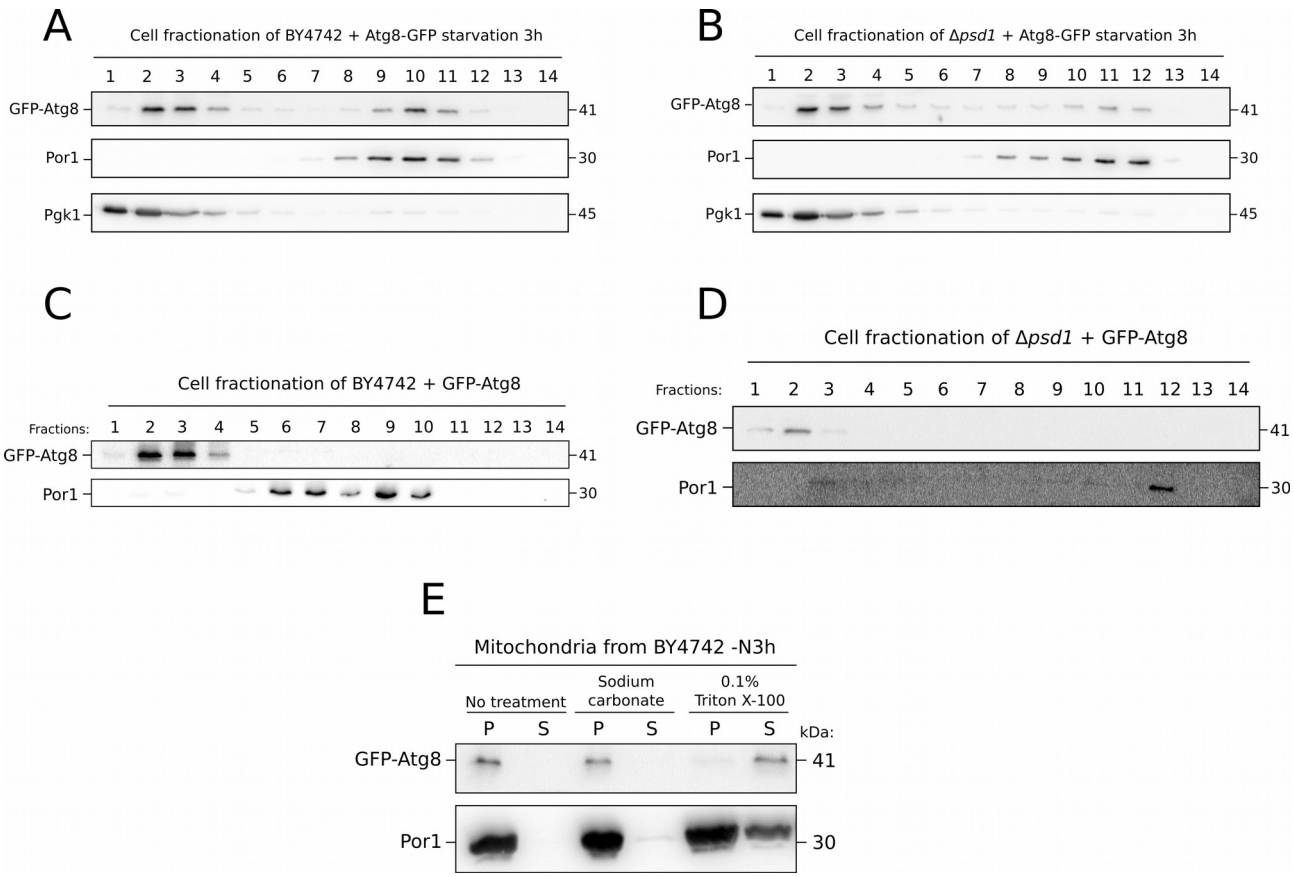

Figure S4: Study of GFP-Atg8 localization by cell fractionation. BY4742 and *Δpsd1* cells expressing GFP-Atg8 were grown in lactate-containing medium (**A**, **B**) or a glucose-containing medium (**C**, **D**) until a mid-exponential phase of growth and submitted to 3 hours of nitrogen starvation. Then, cells were harvested, lysed and cell lysates were separated in a 10-60% OptiprepTM density gradient. Fractions were collected after centrifugation and analyzed by western-blots. Anti-GFP antibody was used to visualize GFP-Atg8 and anti-Por1 to detect mitochondria-containing fractions. Pgk1 was used as a cytosolic marker. Each experiment was performed twice. (**E**) Mitochondria, purified from BY4742 cells submitted to 3 hours of nitrogen starvation, were treated with 100 mM sodium carbonate or 0.1% Triton X-100. After centrifugation, pellets (P) and supernatants (S) were analyzed by western-blots.

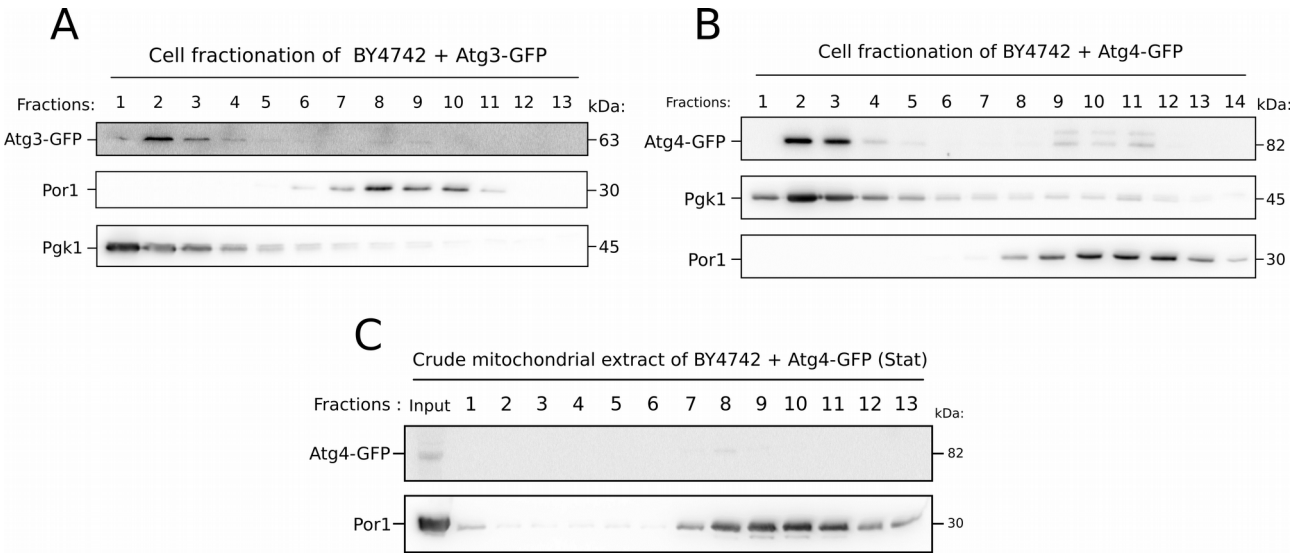

Figure S5: Study of Atg3-GFP and Atg4-GFP localization by cell fractionation. BY4742 cells expressing Atg3-GFP or Atg4-GFP were grown in lactate-containing medium until a mid-exponential phase of growth and submitted to 3 hours of nitrogen starvation (**A**, **B**) or one day of stationary phase of growth (**C**). Then, cells were harvested, lysed and cell lysates were separated in a 10-60% OptiprepTM density gradient. Fractions were collected after centrifugation and analyzed by western-blots. Anti-GFP antibody was used to visualize Atg3-GFP and Atg4-GFP, anti-Por1 to detect mitochondria-containing fractions. Pgk1 was used as a cytosolic marker. Experiments were performed twice.